RED THERMALLY ACTIVATED DELAYED FLUORESCENCE EMITTERS IN ORGANIC LIGHT EMITTING DIODES: A COMPUTATIONAL APPROACH

by

Cansu Dal Kaynak

B.S., Chemistry, Bilkent University, 2010

Submitted to the Institute for Graduate Studies in
Science and Engineering in partial fulfillment of
the requirements for the degree of
Master of Science

Graduate Program in Chemistry

Boğaziçi University

2019

RED THERMALLY ACTIVATED DELAYED FLUORESCENCE EMITTERS IN ORGANIC LIGHT EMITTING DIODES: A COMPUTATIONAL APPROACH

APPROVED BY:

Assoc. Prof. Şaron Çatak .....
(Thesis Supervisor)

Prof. Viktorya Aviyente .....
(Thesis Co-supervisor)

Prof. İlknur Doğan .....

Prof. Nurcan Tüzün .....

DATE OF APPROVAL: 04.10.2019

ACKNOWLEDGEMENTS

Firstly, I would like to express my sincere gratitude to my advisors Prof. Viktorya Aviyente and Assoc. Prof. Şaron Çatak for their continuous support, patience, motivation, and immense knowledge. Their guidance helped me in all the time of research and writing of this thesis. I could not have imagined having better advisors and mentors for my MSc study.

Besides my advisors, I would like to thank the rest of my thesis committee: Prof. Nurcan Tüzün and Prof. İlknur Doğan for their insightful comments and encouragement. I gratefully acknowledge Prof. Antonio Monari (University of Lorraine) and Dr. Seyhan Salman (Clark Atlanta University) for their guidance and support.

Also, I thank my friends in the Computational Chemistry and Biochemistry Group (CCBG) for their kind help and cooperation throughout this period. I thank profusely Deniz Acar for her encouragement, guidance, support and endless friendship.

Last but not the least, I would like to thank my family: my parents, my husband Can Kaynak, my sister Fulya Dal Yöntem and my brother-in-law Bora Yöntem for supporting me spiritually throughout writing this thesis and my life in general.

This study is funded by TUBITAK (Project No: 118Z914) and the computational resources are provided by TUBITAK ULAKBIM High Performance Computing Center.

This thesis is dedicated to the memory of my father, Rifat Dal.

ABSTRACT

RED THERMALLY ACTIVATED DELAYED FLUORESCENCE EMITTERS IN ORGANIC LIGHT EMITTING DIODES: A COMPUTATIONAL APPROACH

This study is a computational analysis of thermally activated delayed fluorescence (TADF) properties for ten molecules emitting red color, together with three molecules having only fluorescent emission. Four different descriptors which are twisting angle (α), low lying singlet triplet energy difference (ΔE_{ST}), triplet states contribution to reverse intersystem crossing (RISC) and Φ_s index with Natural Transition Orbitals (NTOs) were assessed to be able to clearly distinguish TADF emitters from non-TADFs. The geometry optimizations of emitters were performed on ground, singlet and triplet states by Density Functional Theory (DFT) at the M06-2X/6-31G(d) level of theory. Conformation analysis was also carried out to determine the most stable and energetically favorable geometries. Excited state topologies were assessed through the most favorable conformations by Time Dependent Density Functional Theory (TD-DFT) and Tamm-Dancoff Approximation (TDA) at B3LYP/6-31+G(d) by considering solvent effects. Population analysis of NTOs have been performed following TD-DFT and TDA calculations, and Φ_s indices were tabulated by Lowdin and Mulliken charge distributions. As a result of quantum calculation assessments, it has been shown that TADF emitters are well separated from the emitters which perform only fluorescent emission by the four descriptors utilized in this study.This study has revealed the fact that these four descriptors can be further used for suggesting new potential TADF emitters. Thus, developing design strategy for red TADF organic light emitting diodes (OLEDs) can be accelerated.

ÖZET

ORGANİK IŞIK YAYAN DİYOTLARDA KIRMIZI RENKTE IŞIMA YAPAN TERMAL AKTİF GECİKMELİ FLORESAN MATERYALLERİ: HESAPLAMALI YAKLAŞIM

Bu çalışma, kırmızı renkte ışıma yapan, termal aktif gecikmeli floresan (TADF) özelliğine sahip on molekül ile yalnızca floresan emisyonu yapan (TADF olmayan) üç molekülün hesaplamalı analizidir. TADF özelliği gösteren molekülleri, TADF özelliği göstermeyenlerden net olarak ayırabilmek için, bükülme açısı (α), uyarılmış en düşük singlet ve triplet haldeki enerji farkı (ΔE_{ST}), geri yönlü sistemler arası geçişe (RISC) katkıda bulunan uyarılmış triplet haller ile Φ_s değeri ve doğal geçiş orbitallerinden (NTO) oluşan dört farklı tanımlayıcı değerlendirilmiştir. Emisyon yapan moleküllerin geometri optimizasyonları temel, singlet ve triplet hallerinde yoğunluk teorisi fonksiyoneli (DFT) ile M06-2X/6-31G(d)'de yapılmıştır. En kararlı ve enerjisi en düşük geometriyi belirlemek için ayrıca konformasyon analizi gerçekleştirilmiştir. En uygun konformasyonların uyarılmış hal durumları, çözücü etkisini de gözeterek zamana bağlı yoğunluk fonksiyonel teorisi (TD-DFT) ve Tamm-Dancoff yaklaşımı (TDA) ile B3LYP/6-31+G(d)'de analiz edilmiştir. TD-DFT ve TDA hesaplamalarını takiben, NTO popülasyon analizleri yapılarak, Φ_s değerleri Lowdin ve Mulliken yük dağılımı ile raporlanmıştır. Kuantum hesapsal değerlendirmelerin sonucu olarak, bu çalışmada kullanılan dört tanımlayıcı sayesinde TADF özelliği gösteren moleküllerin yalnızca floresan ışıması yapan moleküllerden çok iyi şekilde ayrıştığı görülmüştür. Bu çalışma, yeni potansiyel TADF moleküllerinin önerilmesinde dört tanımlayıcının kullanılabileceğini ortaya koymuştur. Bu sayede kırmızı TADF organik ışık yayan diyotların (OLED) tasarım stratejisinin geliştirilmesinde ivmelenme mümkün olabilecektir.

TABLE OF CONTENTS

LIST OF FIGURES

LIST OF TABLES

LIST OF SYMBOLS

ΔE_{ST}	Singlet triplet energy difference
Φ_{TADF}	TADF quantum yield
Φ_p	Phosphorescence quantum yield
Φ_f	Fluorescence quantum yield
k_p	Phosphorescence rate constant
$\rho(x)$	Electron density
v(r)	External potential
$T[\rho]$	Kinetic energy of interacting electrons
$V_{ee}[\rho]$	Energy of interelectronic interaction
$T_s[\rho]$	Kinetic energy of the non-interacting electrons
$J[\rho]$	Coulomb energy
$E_{xc}[\rho]$	Exchange-correlation energy functional
$E_x[\rho]$	Exchange functional
$E_c[\rho]$	Correlation functional
$\rho(r)$	Ground state density
$F[\rho]$	Functional containing kinetic energy and electron-electron interaction energy
μ	Lagrange multiplier, chemical potential
V_{eff}	Energy functional of non-interacting particle system in external potential
H_{eff}	Hamiltonian operator
$\rho(r,t)$	Time dependent one-body density
$v_{ext}(r,t)$	Time dependent one-body potential
$v_{xc}(r,t)$	Time dependent exchange-correlation potential
$\Psi(0)$	Initial interacting wavefunction
$\Phi(0)$	Initial Kohn-Sham wavefunction
$\hat{H}(t)$	Time dependent Hamiltonian operator
r_i	Particle coordinate
t	Time

P	Polarization propagator
I	Electron-hole interaction kernel
v	Coulomb kernel
W	Static (instantaneous) screened interaction
ζ	Valence zeta basis sets
$\{r_a\}$	Cartesian coordinates
S	Surface of the solute
γ	Surface tension coefficient
Φ_v	Electrostatic potential computed in vacuum
Φ_s	Electrostatic potential computed in the solvent
Q_a	Charge of atom a
$\Phi(r)$	Electrostatic potential
$\epsilon(r)$	Dielectric constant
$\overline{k}(r)$	Debye-Hückel screening factor
$\rho(r)$	Fixed charge density of the solute
Φ_s index	Quantitative topological descriptor

LIST OF ACRONYMS/ABBREVIATIONS

EJ	Exajoule
LCDs	Liquid Crystal Displays
LEDs	Light Emitting Diodes
OLEDs	Organic Light Emitting Diodes
EQE	External Quantum Efficiency
PhOLEDs	Phosphorescence OLEDs
ISC	Inter System Crossing
TTA	Triplet-Triplet Annihilation
IQE	Internal Quantum Efficiency
TADF	Thermally Activated Delayed Fluorescence
RISC	Reverse Intersystem Crossing
FMOs	Frontier Molecular Orbitals
D	Donor
A	Acceptor
HOMOs	Highest Occupied Molecular Orbitals
LUMO	Lowest Unoccupied Molecular Orbitals
PLQYs	Photoluminescence Quantum Yields
FWHM	Full Width at Half Maximum
IC	Internal Conversion
DFT	Density Functional Theory
TD-DFT	Time Dependent Density Functional Theory
HF	Hartree–Fock
TDA	Tamm–Dancoff Approximation
TD-HF	Time-Dependent Hartree–Fock
BSE	Bethe-Salpeter Equation
CSM	Continuum Solvation Model
PCM	Polarizable Continuum Model
COSMO	Conductor-like Screening Model

PB	Poisson-Boltzmann
NTOs	Natural Transition Orbitals
THF	Tetrahydrofuran
CT	Charge Transfer
SOC	Spin–Orbit Coupling

1. INTRODUCTION

One of the most common problems that researchers are coping with in recent centuries is to build a system with the best performance by solving "trilemma, 3E", i.e. to find out how to have a growth in economy without depleting energy and other resources and without harming the environment. An "energy system" is used to transform energy from one form to another useful form such as mechanical, electrical, thermal, light, and due to its complexity, it is difficult to have 100% efficient energy at low cost in an environment friendly structure [1]. Regarding the importance of this 3E, Sustainable Development Goals have been determined as affordable and non-polluting energy, sustainable cities and communities, or climate action. By considering the demand of today's modern life for sustainability, 3E is much more essential than ever before [2].

Energy is an indispensable necessity for technology. Without energy, the society would face with difficulties to maintain their lives, for e.g., a 24-h shortage in electricity supplies to a city causes to stop working of computers, obstruct having hospital care, complicate reaching clean water sources and leave people in darkness. It shows that how society is dependent on useful form of energy. The growth in population more than 2% leads to more and more energy need. Besides, well developed countries (25% of world's population) require more energy supply (around 75% of world's energy demand) due to enhanced lifestyle and technology [3]. In 2008, energy consumption was 514 EJ (EJ = exajoule = 1018 J) from all sources that more than 80% of them belong to fossil fuels, and in 2050, an increase of around 800 EJ in world energy use is expected in a business-as-usual world [4].

Economy is directly or indirectly dependent on energy use. Fossil fuels which are the most common source of energy use make economy unbalanced causing to debt problems between countries [5]. Production costs are also another effect of energy consumption on economy. For economic growth targets, technological development is highly required since it is recognized as crucial to overcome production costs by increasing efficiency [6]. Improved energy yield promotes local sustainability and it

provides undeniable advantage, even against countries which are rich in fossil fuel sources, depending on low production cost in energy-intensive sectors [7].

Environmental consideration is another aspect of energy supply and use. Global warming, air pollution, acid precipitation, ozone depletion, forest destruction and emission of radioactive substances are energy related environmental issues which must be considered while designing much better clean alternative energy systems. One of the major solutions to the energy shortage which is likely to happen in future is to use more renewable energy sources and technologies [3].

Issues about energy insecurity, economic growth and global climate change can be overcome by immediate development in low carbon technologies and management. There is a broad range of ongoing projects for technological development, but they are not at desired speed because of some financial, commercial, technological and regulatory related difficulties.

Display technology has a tremendous effect on today's modern life, and it shapes the lifestyle of people. The energy system used in this technology transforms electrical energy into light. Currently, liquid crystal displays (LCDs) are much widely used technology which have applications in smartphones, tablets, computers, televisions, projectors etc. However, light emitting diodes (LEDs) and organic light emitting diodes (OLEDs) have developed rapidly in recent years and they found a remarkable market, especially in small-sized displays [8].

OLEDs are good candidates to fulfill lighting needs of society with less production costs and to reduce carbon emission with less energy consumption. In addition to their superior color quality, OLED displays have much thinner design than LCDs and LEDs due to their composition with less layers and no backlight requirement. This advantageous structure in OLEDs requires lower voltage which means less energy consumption and they provide much flexible devices with more efficient viewing angles. In addition, temperature can be controlled in OLEDs much easily because heat formation is dispersed, and heat flux is small due to their thin design and plane light source. Besides,

LEDs which are inorganic form of OLEDs, generate high luminescence with high heat flux leading to thermal degradation. Due to this, device is covered by organic resin and necessity to have large number of LED tips on flat surfaces causes high costs [9].

Electroluminescence is light emission when electricity is applied through a solid. OLEDs are designed as thin multi-layer devices consisting of foil, film or plate, an electrode layer, layers of active substances which are combination of host and emitter, a counter electrode layer (transparent to light) and protective barrier layer. When low voltage (around 2.5 – 20 V) is applied to electrodes, electric field in active layers becomes so high (around 105 – 107 V/cm) since low voltage is dispersed through thin active layers (around 10 Å to 100 nm). This high electric field facilitates charge injection through electrode to active layers. Holes which are injected from anode meet and recombine in emission layer with the electrons which are injected from the cathode. At emission layer, recombination energy is released, and the molecule is excited. Molecules called emitters in OLEDs finally release all excess excitation energy as photons (light) [10]. A typical OLED structure together with its photograph and energy-level diagram are shown in Fig 1.1. [11].

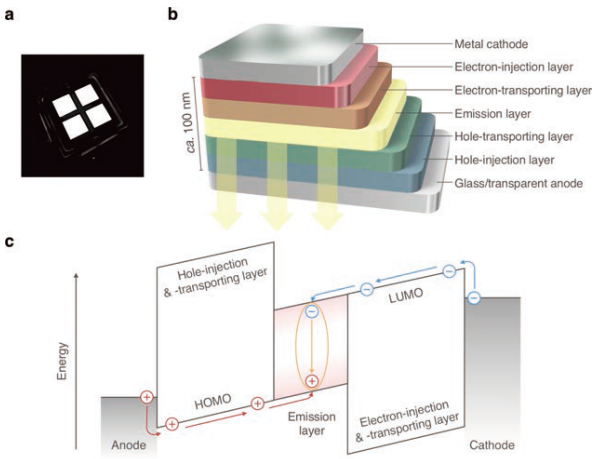

Figure 1.1. (a) Picture of an OLED. (b) Device structure of typical OLEDs. (c) Schematic energy-level diagram of typical OLEDs.

Spin statistics determine the suitable multiplicity at excited state after recombination by spin-half particles of injected carriers. Accordingly, 25% of this recombination go to singlet excited state while 75% of the excitons are expected to be at triplet state. Conventional first-generation fluorescent OLEDs utilize only singlet excitons (25% probability) so electrical power is lost generating dark triplet state excitons (75% probability). Thus, only 5-7.5% of external quantum efficiency (EQE) is achieved by these fluorescent OLED devices and this is not satisfactory for industrial applications [12].

Second-generation phosphorescence OLEDs (PhOLEDs) were discovered as breakthrough technology which are better alternative to fluorescent OLEDs with 100% exciton utilization from both triplet and singlet states. Emitters consisting of heavy transition metals in PhOLEDs provide large spin-orbit coupling leading to intersystem crossing (ISC) of singlet excitons to the relevant triplets. Thus, highest EQE in PhOLEDs can reach up to 20-30%. However, these commercial PhOLEDs utilized from organometallic phosphors have critical drawbacks such as toxicity, rare availability of these metals, production costs, device stability etc. [12].

Triplet-triplet annihilation (TTA, also known as P-typed delayed fluorescence) is another triplet harvesting method which can be seen in pure organic fluorescent probes. When compared to fluorescence, the rate constant of emission for TTA is not high as it depends on rate of formation of triplet excitons. In terms of efficiency, some reports indicated that pure organic chromophores using TTA showed better results than those of fluorescent OLEDs, however, they are still not better alternatives than PhOLEDs having 100% internal quantum efficiency (IQE) since their IQE is limited to 62.5% [12].

Thermally activated delayed fluorescence (TADF) provides 100% exciton utilization by reverse intersystem crossing (RISC) of triplet excitons to singlet state as delayed fluorescence followed by regular fluorescence. Proper organic chromophore having sufficiently small (less than 0.1 eV) singlet triplet energy difference (ΔE_{ST}) shows TADF property when ambient temperature is available as thermal energy ($\approx$ 25.6 meV at 298 K). TADF was firstly shown by deoxygenated solution of eosin in glycerol and ethanol

at room temperature [12]. Three generations of OLEDs are shown schematically in Fig 1.2.

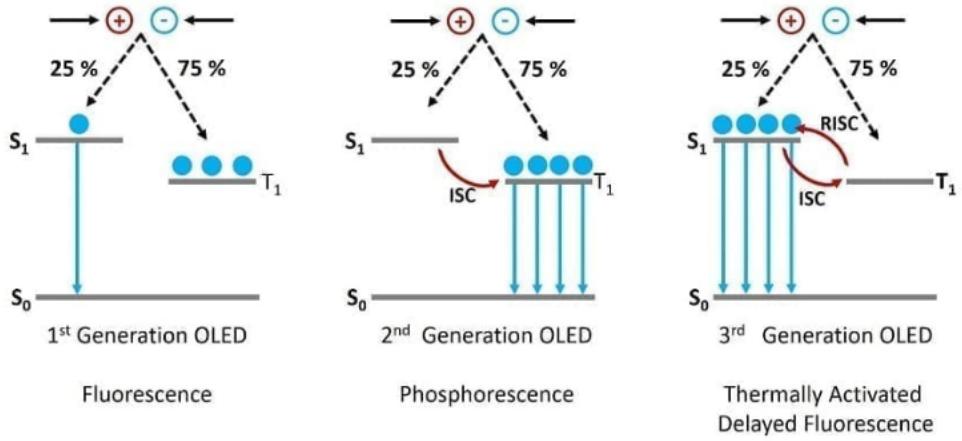

Figure 1.2. Schematic representation of three different generations of OLEDs.

TADF and prompt fluorescence have similar wavelengths in their emission spectrum however, lifetime differs since lifetime of TADF is much closer to that of triplets. Arhenius type equation below expresses the rate constant which is temperature dependent, A is frequency factor and R is the gas constant in this equation.

$$k_{TADF} = Aexp(-\frac{\Delta E_{ST}}{RT}) \tag{1.1}$$

By using it, the ratio of quantum yields of TADF (Φ_{TADF}) and phosphorescence (ϕ_p) can be demonstrated as the following

$$\frac{\Phi_{TADF}}{\Phi_p} = \Phi_f \frac{A}{k_p} exp(-\frac{\Delta E_{ST}}{RT}) \tag{1.2}$$

where Φ_f is fluorescence quantum yield and k_p is phosphorescence rate constant. This implies that triplet generation yield and triplet quenching process are not dependent on $\frac{\Phi_{TADF}}{\Phi_p}$ ratio [12].

Quantum chemical calculations determine that ΔE_{ST} is approximately double the electron exchange energy and it is shown by the following equation

$$\begin{aligned} J &= \int\int (\phi)^1(\phi^*)^1 \frac{e^2}{r_{12}} (\phi^*)^1(\phi)^1 d\tau_1 d\tau_2 \\ &= \int\int \frac{[(\phi)^1(\phi^*)^1 e][e(\phi^*)^1(\phi)^1]}{r_{12}} d\tau_1 d\tau_2 \end{aligned} \tag{1.3}$$

where ϕ and ϕ^* are wavefunctions belonging to ground and excited states. TADF emitters should have small J values since J is supposed to be close to Coulombic repulsion interaction between two equal charge densities ($\phi\phi^* e$). Therefore, small overlap integral $\langle\phi|\phi^*\rangle$ implies small J and ΔE_{ST} and it can be obtained through localization of frontier molecular orbitals (FMOs). In light of this, while designing emitters to have TADF character, donor (D) and acceptor (A) should be attached to each other appropriately in sterically crowded geometry by minimizing overlap between highest occupied molecular orbitals (HOMOs) and lowest unoccupied molecular orbitals (LUMO) [12]. This is crucial to minimize the barrier for charge injection and to control the recombination region in device while achieving better lifetime and high photoluminescence quantum yields (PLQYs) which show device efficiency [13].

TADF property can be controlled by managing donor and acceptor moieties. Different design strategies for TADF emitters are available in literature like donor-acceptor, donor-acceptor-donor and donor-bridge-acceptor-bridge-donor as much complex one. In addition, substitution of donor and acceptor plays important role to obtain better TADF emitters. It has been shown that ortho, meta and para substitution of donor and acceptor in common phenyl core changed EQE, efficiency and lifetime of TADF OLEDs [14]. Conformational changes are another consideration for TADF emitters as they change their conformations to make a new stabilized dipolar state or exciplex (a concept that donor and acceptor are not chemically bounded) after optical excitation. This state can arise directly following excitation or it may sequentially occur within locally excited states. Twisting, bending or planarization of D and A bond in excited state lead to spatial molecular conformations which can be stabilized by polarity of solvent and temperature [15]. It has been shown that highly twisted

donor-acceptor structure favors RISC for TADF emitters. However, it must be noted that more twisted structures cause more relaxation leading to red shifting in emission spectra [16].

Parameters used to describe the favorable OLED devices are EQE, color purity, lifetime and efficiency roll-off. EQE is subject to PLQY, color purity depends on full width at half maximum (FWHM), lifetime changes according to the stability of material and efficiency roll-off is governed by lifetime of delayed fluorescence in control of ΔE_{ST}. High EQE, good color purity, long lifetime and small efficiency roll-off must be obtained for better TADF OLEDs [17]. Main disadvantage of TADF OLEDs is shorter lifetime due to degradation of organic molecules and it changes depending on the emitters showing different colors in OLEDs that are red and green OLEDs (46,000 to 230,000 hours) have longer lifetime than blue OLEDs (up to around 14,000 hours) [10]. In addition, long lifetime of triplet excitons causes severe roll-off at high current density by creating accumulation of concentration. Therefore, in current applications, doped OLEDs, i.e. including host in emission layer, are used to eliminate this roll-off and to provide higher efficiency, however, they increase production costs when compared to non-doped applications [18]. Regarding this, researchers are working on a way to create better non-doped emitter which can boost OLED efficiency by itself or to develop efficient host and emitter which will promote efficiency in device as well as lifetime while having relatively low cost [12].

The intense literature about new TADF emitters demonstrates that the interest on the design of new TADF molecules by considering structure-property relationship deeply rises each day. These efforts lead to increase in progress for better TADF molecules however, simple design rules serve to only specific property like emission and absorption wavelength, so they are not enough to control all photophysical properties. In addition, conflictive requirements of efficient TADF emitters such as having a large radiative rate with a small ΔE_{ST} make the case much more difficult. Minimization of exchange energy causes small singlet-triplet gap, but this leads also to smaller radiative rates. The design development can be accelerated by computational methods which have a great potential for monitoring potential emitters. Regarding this, Gomez et al.

explored a chemical space of 1.6 million molecules by unique virtual screening method, however, these kinds of approaches are not successful due to some defined criteria which are valid only for specific molecular properties. Therefore, descriptors for designing efficient TADF emitters must be identified and optimized by understanding the TADF mechanism in detail [19].

Different design strategies can be required for TADF emitters showing distinct colors (green, blue, red) in OLEDs due to their energies. While efficient RISC process and high fluorescence quantum yield can be achieved much easily for blue and green TADF emitters, it is much difficult to overcome increased internal conversion (IC) rate from singlet to ground state against fluorescence rate in red molecules and this IC process leads to huge energy loss. For example, AQ-DMAC which is one of the red TADF molecule having highly twisted D-A structure demonstrates small ΔE_{ST} of 0.08 eV however, it cannot be used as an emitter since its IC rate is 10 times higher than its fluorescence rate. Therefore, for efficient red TADF emitters, in 2014, Adachi et al. suggested a novel structure, D-phenyl-A, by binding phenyl as bridge and AQ-TPA with this structure achieved a maximum EQE of 12.5% by exhibiting less than a quarter value in its IC rate than its fluorescence rate. However, when the conjugation between D and A moieties is enhanced, larger ΔE_{ST} value which is higher than 0.17 eV is obtained by weakening RISC and causing to energy loss from triplet state. In the past several years, greater progress has been achieved in blue and green TADF OLEDs that their EQE has reached to more than 20% however, maximum EQE for recent red TADF OLEDs is 17.5% which was obtained by HAP-3TPA. As it is even lower than theoretical ceiling of 20% EQE, further development is highly required for red TADF emitters in OLEDs [20].

2. METHODOLOGY

2.1. Density Functional Theory

Density Functional Theory (DFT) is used to carry out high-speed calculations of many-electron systems by representing the potential as the functional of the electron density. This concept was firstly suggested by Thomas-Fermi in 1927 and his theorem was revived by Hohenberg and Kohn (Hohenberg-Kohn theorem) in 1964. This theorem consists of two supplementary theorems for non-degenerate ground electronic states [21].

The first theorem is about external potentials which are described by the electron density corresponding to the nuclear–electron interaction potentials when an electromagnetic field is not available. The second theorem is about the variational principle that Hamiltonian operator is in place to represent electron density while determining (local) minimum energy [21].

The electron density $\rho(x)$ is

$$\rho(x) = N \int ... \int |\Psi(x_1, x_2, ...x_n)|^2 dx_1, dx_2, ...dx_n \tag{2.1}$$

x in here represents coordinates of electrons as spin and spatial. The energy as a function of electron density can be written as

$$E[\rho] = \int v(r)\rho(r)dr + T[\rho] + V_{ee}[\rho] \tag{2.2}$$

v(r) here is the external potential, $T[\rho]$ is the kinetic energy of interacting electrons and $V_{ee}[\rho]$ is the energy of interelectronic interaction. Then, the electronic energy can

be rewritten as

$$E[\rho] = \int v(r)\rho(r)dr + T_s[\rho] + J[\rho] + E_{xc}[\rho] \tag{2.3}$$

where $T_s[\rho]$ is the kinetic energy of the non-interacting electrons, $J[\rho]$ is the Coulomb energy and $E_{xc}[\rho]$ is the exchange-correlation energy functional. $E_{xc}[\rho]$ can be represented as

$$E_{xc}[\rho] = E_x[\rho] + E_c[\rho] \tag{2.4}$$

where $E_x[\rho]$ is the exchange functional representing the interaction between electrons with same spin and $E_c[\rho]$ is the correlation functional indicating the interaction between opposite spins of electrons. The exchange-correlation functional consists of a kinetic energy term which originates from the difference in energy between the interacting and non-interacting electron systems. The favorable energy contributions in here are the kinetic energy term as freedom and exchange-correlation energy which represents the change of opposite spin electrons. Total electronic energy was disfavored by the unfavorable electron-electron repulsion energy defined as Coulomb energy term [22].

Kohn–Sham theorem is used to visualize the many-particle problem onto a system including non-interacting electrons with the same ground state density $\rho(r)$ as the original many-particle system [23]. The total energy functional can be shown as

$$E[\rho] = F[\rho] + \int d^3r V_{ext}(r)\rho(r) \tag{2.5}$$

where $F[\rho]$ is the universal functional. It is written as

$$F[\rho] = T_s[\rho] + \frac{1}{2}\int d^3r' \frac{\rho(r)\rho(r')}{|r - r'|} + E_{xc}[\rho] \tag{2.6}$$

Variation of the energy functional can be written with $F[\rho]$ for many particle systems

as the following when $\delta E[\rho] = 0$ is defined

$$\mu = \frac{\delta E[\rho]}{\delta \rho(r)} = V_{ext} + \int d^3r d^3r' \frac{\rho(r')}{|r - r'|} + \frac{\delta T_s[\rho]}{\delta \rho(r)} + \frac{\delta E_{xc}[\rho]}{\delta \rho(r)} \tag{2.7}$$

where μ is Lagrange multiplier which is also called as the chemical potential. Energy functional of non-interacting particle system in external potential (V_{eff}) is defined as

$$E[\rho] = T_s[\rho] + \int d^3r V_{eff}(r)\rho(r) \tag{2.8}$$

and variation gives

$$\mu = \frac{\delta E[\rho]}{\delta \rho(r)} = \frac{\delta T_s[\rho]}{\delta \rho(r)} + V_{eff} \tag{2.9}$$

(2.7) can be described again by taking (2.9) into account as the following

$$V_{eff} = V_{ext} + \int d^3r' \frac{\rho(r)}{|r - r'|} + \frac{\delta E_{xc}[\rho]}{\delta \rho(r)} \tag{2.10}$$

V_{eff} is an effective external potential where the non-interacting electrons are moving. Exchange-correlation potential, in this equation, is

$$V_{xc} = \frac{\delta E_{xc}[\rho]}{\delta \rho(r)} \tag{2.11}$$

V_{eff} provides the many particle problem to convert into a single particle formulation. Then, Hamiltonian (H_{eff}) in (2.8) is determined as

$$H_{eff} = -\frac{1}{2} \bigtriangledown^2 + V_{eff}(r) \tag{2.12}$$

It gives Schrödinger-like equation which is also known as Kohn–Sham (KS) equations

$$H_{eff}(r)\psi_i(r) = [-\frac{1}{2} \bigtriangledown^2 + V_{eff}(r)]\psi_i(r) = \epsilon_i \psi_i(r) \tag{2.13}$$

Solutions of this equation are known as Kohn–Sham eigenvalues and eigenfunctions. The ground state density is stated as sum of N lowest eigenstates of H_{eff}

$$\rho(r) = \sum_{i=1}^{N} |\psi_i(r)|^2 \tag{2.14}$$

As H_{eff} is directly linked with $\rho(r)$, coupling between N one-electron equations in (2.13) are generated by (2.14). T_s (the kinetic energy term) can then be calculated by Kohn–Sham equation

$$T_s = \sum_{i=1}^{N} \langle \psi_i | -\frac{1}{2} \bigtriangledown^2 | \psi_i \rangle = \sum_{i=1}^{N} \epsilon_i - \int d^3 r V_{eff}(r) \rho(r) \tag{2.15}$$

Finally, the total energy can be expressed as

$$E = \sum_{i=1}^{N} \epsilon_i - \frac{1}{2} \int d^3 r d^3 r' \frac{\rho(r)\rho(r')}{|r - r'|} - \int d^3 r V_{xc}[\rho]\rho(r) + E_{xc}[\rho] \tag{2.16}$$

Ground state properties of many-electron systems can only be calculated accurately with the Kohn–Sham approach outlined above which compares both experimental data and the results of much more involved configuration interaction calculations [23].

2.2. Time Dependent Density Functional Theory

Time-Dependent Density Functional Theory (TD-DFT) has been used as an expansion of DFT in the account of time dependent nature of electromagnetic waves for treatment of excited states electronically (light matter interactions). It is an accurate solution to TD Schrödinger equation and due to its great accuracy and cpu-effort ratio, it becomes more popular and widely used method [24].

One-to-one correspondence is available among with one-body densities $\rho(r, t)$ and one-body potentials $v_{ext}(r, t)$ which are timely dependent for a given initial state within certain general circumstances. One time-dependent potential can constitute evolution of the density. This statement is the time-dependent version of Hohenberg-Kohn

theorem. Thus, an artificial system where non-interacting electrons are moving in a time-dependent effective potential can be described in such a way that its density becomes accurately same with that in the real system. This effective potential is called time-dependent Kohn-Sham potential. As in the ground state DFT theory, it includes Hartree potential as external and the exchange-correlation potential, $v_{xc}(r,t)$, which is a functional of the density, $\rho(r,t)$, the initial interacting wavefunction, $\Psi(0)$ and the initial Kohn-Sham wavefunction, $\Phi(0)$ [25].

Time-dependent Schrödinger equation governs the evolution of the wavefunction where $\psi(0)$ is given

$$\hat{H}(t)\psi(t) = i\frac{d\psi(t)}{dt} \tag{2.17}$$

here $\hat{H}(t)$ is the Hamiltonian operator. The initial wavefunction should be designated since this is a first-order differential in time. N non-relativistic electrons which interact as a result of Coulomb repulsion within a time-dependent external potential are considered. Kinetic energy is written as

$$\hat{T} = -\frac{1}{2}\sum_{i=1}^{N} \nabla_i^2 \tag{2.18}$$

Label i here indicates the particle coordinates r_i. The electron-electron repulsion is defined as

$$\hat{V}_{ee} = \frac{1}{2}\sum_{i\neq 1}^{N} \frac{1}{|r_i - r_j|} \tag{2.19}$$

And, one-body potential is described as

$$\hat{V}_{ext} = \sum_{i=1}^{N} v_{ext}(r_i, t) \tag{2.20}$$

One-particle density of the system changes, as it evolves from an initial point by time

(t = 0). This electron density is defined as

$$\rho(r,t) = N \int d^3r_2 ... \int d^3r_N |\psi(r, r_2, ..., r_N, t)|^2 \tag{2.21}$$

where $\rho(r,t)d^3r$ is the probability of any electron found in d^3r area around r at time t. It is normalized to the number of electrons

$$\int d^3r \rho(r,t) = N \tag{2.22}$$

2.3. Tamm Dancoff Approximation

Hartree–Fock (HF) theory and Kohn-Sham density functional theory have some difficulties for obtaining reliable response in triplet state calculations. They both experience some instability issues while calculating triplet properties, especially in DFT, it is much complicated since stability depends on the choice of exchange-correlation functional. By applying Tamm–Dancoff approximation (TDA) to time-dependent Hartree–Fock (TD-HF) and TD-DFT for calculation of triplet excitation energies, problems associated with triplet instabilities are overcome and computationally more tractable response equations are obtained [26].

Bethe-Salpeter equation (BSE) is used to calculate linear optical properties precisely. By including a convenient product basis for electron-hole pairs, this equation re-forms the complex non-Hermitian eigenvalue issue which is hard to solve by using standard eigenvalue operations. Therefore, it is a general application to avoid problematic coupling between positive and negative frequency branches by minimizing it to a Hermitian eigenvalue problem which is known as TDA [27].

The excitation energies are described by calculating polarization propagator and this requires diagonalization of a large matrix in which its dimension is equivalent to multiplication of the number of occupied states with those of unoccupied states. After

some alterations, BSE can be converted into a Dyson-like equation

$$P = P_0 + P_0 I P \tag{2.23}$$

P(1,2,3,4) is the polarization propagator which is four-point time-ordered and I is the electron-hole interaction kernel. Space and time points, $1 = (r_1, t_1)$ is used as common notation.

(2.23) is like the response equation for χ^{TD} from TD-DFT, where P is considered as generalized linear density matrix response function to a nonlocal perturbation. Apparently, alteration of these four-point quantities is much more involved compared to the simpler TD-DFT two-point quantities. In common use, P(1,2,3,4) is described in a suitable two-orbital basis which is formed by all relevant combinations of electron and hole pairs. In addition, I is approximated by the Coulomb kernel v and a static (instantaneous) screened interaction W. This static approximation is implemented for simplification of the calculations [27].

2.4. Basis Sets

In relativistic quantum mechanics, the fundamental principles are based on the equations of Schrödinger or Dirac-Coulomb. Since these equations cannot be solved by conventional mathematics manually, iterative numerical computations are utilized by adapting the radial part of the wavefunction or electronic density with mathematical functions which are known as basis sets. In application, three different basis sets (Slater, Gaussian, and plane-wave) are commonly used [28]. Among them, Gaussian basis sets are much easier to calculate [29]. In practice, most widely used basis sets are 3-21G, 6-21G, 6-31+G and 6-311G*.

The first number in the basis set represents core functions while the numbers after hyphen are for valence functions. Since valence electrons are so important during bonding process, there are multiple functions representing each valence atomic orbital in the basis sets. They are the valence double, triple, quadruple-zeta (ζ) basis sets.

Polarization functions expressed by an asterisk, *, is the most common addition to minimal basis sets. They can also be expressed with two asterisks, **, which mean that polarization functions are added to light atoms (hydrogen and helium) as well. When polarization is available, p-function is also added to basis set and it provides some extra flexibility within the basis set. Similarly, d-type functions can be included into a basis set with valence p orbitals and f-functions with d-type orbitals [30].

Diffuse functions are another common inclusion into basis sets, and they are expressed in Pople-type sets by a plus sign, +. + is added for heavy atoms and ++ signs are used for light atoms (hydrogen and helium). When anions and other large, "soft" molecular systems are in consideration, these diffuse functions become more significant [30].

2.5. Continuum Solvation Models

Continuum solvation models (CSMs) like polarizable continuum model (PCM) and the conductor-like screening model (COSMO) are efficient and exact tools for demonstration of solvation effects in quantum chemical calculations. A cavity is presented around relevant solute molecule in all these models where a dielectric continuum is applied. By polarization of this continuum, the molecular electric field generated by nuclei and electron distribution is screened. As a common knowledge from basic electrostatics, polarization effect can be defined by surface charge density since it takes place on the boundary. As the only boundary is the solute interface, it is advantageous that all effect can be determined by monitoring the charges obtained on the surface, especially when an infinite extended continuum is assumed. Widely ranged polarization, then, can be identified without having any issue due to finite size, by a local system including solute together with cavity surface [31].

Continuum electrostatics in macro system are based on Poisson-Boltzmann (PB) equation where the solvent is defined as a featureless dielectric material. The solvation free energy of a molecular solute found in configuration fixed with Cartesian coordinates $\{r_a\}$ can be described in an order since the reversible thermodynamics take place

sequentially when it is immersed into a polar solvent having mobile ions. Firstly, neutral solute is immersed into solvent and then electrostatic interactions between solute and solvent are initiated [32]. Finally, solvation free energy is defined as the sum of nonpolar contributions (np) consisting of formation energy for cavity in solvent and solvent-solute van der Waals interaction (dispersion and repulsion) energy and electrostatic contributions (elec)

$$\Delta G_{solv} = \Delta G_{np} + \Delta G_{elec} \tag{2.24}$$

Solvation free energy with nonpolar contribution is described with the surface of the solute, S, and a surface tension coefficient, γ

$$\Delta G_{np} = \gamma S \tag{2.25}$$

Electrostatic potential computed in vacuum (Φ_v) is subtracted from the total electrostatic potential computed in the solvent (Φ_s) to calculate electrostatic contribution to the solvation free energy

$$\Delta G_{elec} = \frac{1}{2} \sum_a Q_a [\Phi_s(r_a) - \Phi_v(r_a)] \tag{2.26}$$

Q_a here is the charge of atom a. Electrostatic potential $\Phi(r)$ in this formula is calculated by following Linear Poisson- Boltzmann (PB) equation

$$\bigtriangledown[\epsilon(r) \bigtriangledown \Phi(r)] - \overline{k}^2(r)\Phi(r) = -4\pi\rho(r) \tag{2.27}$$

where $\epsilon(r)$ is dielectric constant, $\overline{k}(r)$ is the modified Debye-Hückel screening factor and $\rho(r)$ is the fixed charge density of the solute.

2.6. Φ_s Index

A normalized, dimensionless quantity called as Φ_s is used for computing spatial overlap between hole and particle as a magnitude of the electronic structure reorganization in the first quantitative strategy [33].

$$\Phi_s = \vartheta_x^{-1} \int_{\mathbb{R}^3} dr \sqrt{n_d(r) n_a(r)} \in [0;1]; \vartheta_x = \frac{1}{2} \sum_{q=d,a} \int_{\mathbb{R}^3} dr n_q(r) \tag{2.28}$$

ϑ_x here is a normalization factor which represents detachment/attachment density at every point of space, while $n_q(r)$ is the charge density. Small Φ_s value indicates small overlap between hole and particle as a result of long-range charge transfer. In contrast, larger Φ_s value shows the availability of local transition. It has also been shown that exchange correlation functional can be diagnosed via Φ_s value while doing computational analysis of transition energy with TD-DFT [33].

Effectively displaced charge density is another aspect of quantitative strategy. Figure 2.1 clearly shows the illustration of charge density through transition as well as hole-particle overlap. When overlap is available between densities of hole and particle, positive and negative contribution to density difference is in the first place instead of detachment and attachment. It is calculated by considering the charge density difference between attachment and detachment at all over the space [33]. The following equation can be derived as

$$n_\Delta(r) = n_a(r) - n_d(r), \tag{2.29}$$

by using the following formula

$$m = k_+ - k_- \Rightarrow \gamma^\Delta = MmM^+ = Mk_+M^+ - Mk_-M^+ = \gamma^a - \gamma^d \tag{2.30}$$

$n_\Delta(r)$ here is the density matrix projected to Euclidean space. Thus, displacement

charge density can be stated as

$$n_{\pm}(r) = \frac{1}{2}\{\sqrt{n_{\Delta}^{2}(r) \pm n_{\Delta}(r)}\} \tag{2.31}$$

Computation of normalized displaced charge can be carried out by the following equation, by considering sign of functions instead of transition occupation numbers while executing splitting operation [33].

$$\frac{\vartheta_{x}^{-1}}{2} \sum_{s=+,-} \int_{\mathbb{R}^3} dr n_{s}(r) = \tilde{\varphi} \in [0;1] \tag{2.32}$$

$n_s(r)$ is the density which considers splitting. Negative and positive contribution to density difference are not the only metric, addition of splitting transition occupation numbers and computation of detachment and attachment overlap are also required to finalize general quantum metric for charge transfer as following

$$\psi = 2\varphi^{-1} \underbrace{arctan(\frac{\varphi_s}{\tilde{\varphi}})}_{\theta_s} = \frac{2\theta_s}{\varphi} \in [0;1] \tag{2.33}$$

where Φ_s represents the localization of charge transfer while φ is related to charge transfer amount formed during transition. Φ_s and φ here are normalized and dimensionless. $2\pi^{-1}$ factor in this equation is used to be sure about normalized φ angle formed as a result of joint projection of Φ_s and φ in a complicated plane (φ is accepted on real axis while Φ_s is on imaginary axis). This kind of projection is described by a θ_s angle on the real axis, considering the values ranging from 0 to $\pi/2$ [33].

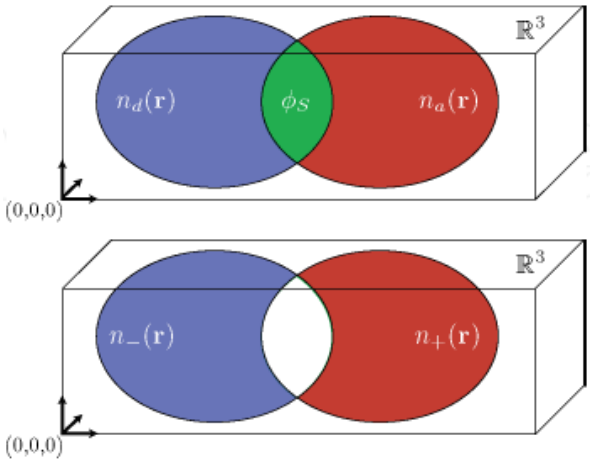

Figure 2.1. Drawing of the complementarity between Φ_s and φ.

3. AIM OF THE STUDY

In this study, a quantum computational investigation of a range of red TADF emitters, which have generally lower EQE values than other TADF OLEDs having different color regions, was performed to understand the relationship between molecular structures and their photophysical properties. TADF properties of these red TADF emitters were examined by categorizing them to subgroups such as D-A-D or A-D-A and D-X-A-X-D which include additional bridge.

In addition, red fluorescent (non-TADF) emitters were utilized as cross comparison group to understand TADF mechanism in detail for being able to suggest potential TADF molecular structures and accelerate design development of TADF OLEDs. The different groups of molecular structures as D-A-D and D-A were investigated as non-TADF emitters.

To clearly distinguish TADF emitters from non-TADFs, four different descriptors called twisting angle (α), low lying singlet triplet energy difference (ΔE_{ST}), triplet states contribution to RISC and Φ_s index with natural transition orbitals (NTOs) were identified in this study. The main purpose of the work is to suggest new potential emitters to develop more efficient red TADF OLEDs. While achieving this goal, the structural requirements of materials exhibiting TADF will be rationalized.

4. RESULTS AND DISCUSSION

4.1. Background

TADF materials used in OLED devices have a great interest since they were firstly reported by Adachi et Al. in 2011 [34] due to their special exciton harvesting mechanism which can easily achieve 100% of IQE. Since then, considerable efforts have been given to understand the reasons behind these special TADF characteristics which make them better alternatives to fluorescent or phosphorescent emitters used in OLEDs [35].

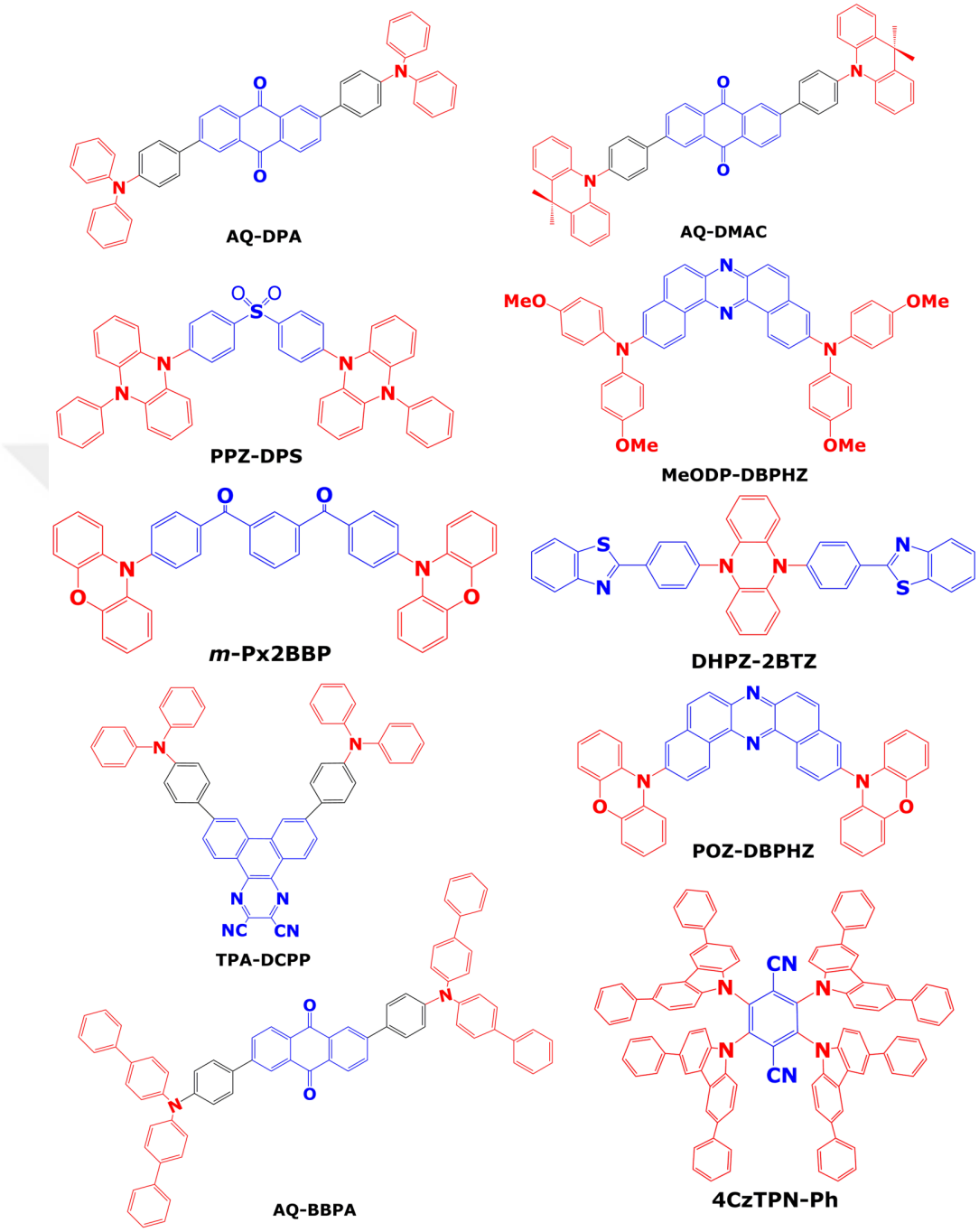

Figure 4.1. 2D structures of TADF emitters utilized in this study. Red color identifies donors while blue color shows acceptor units.

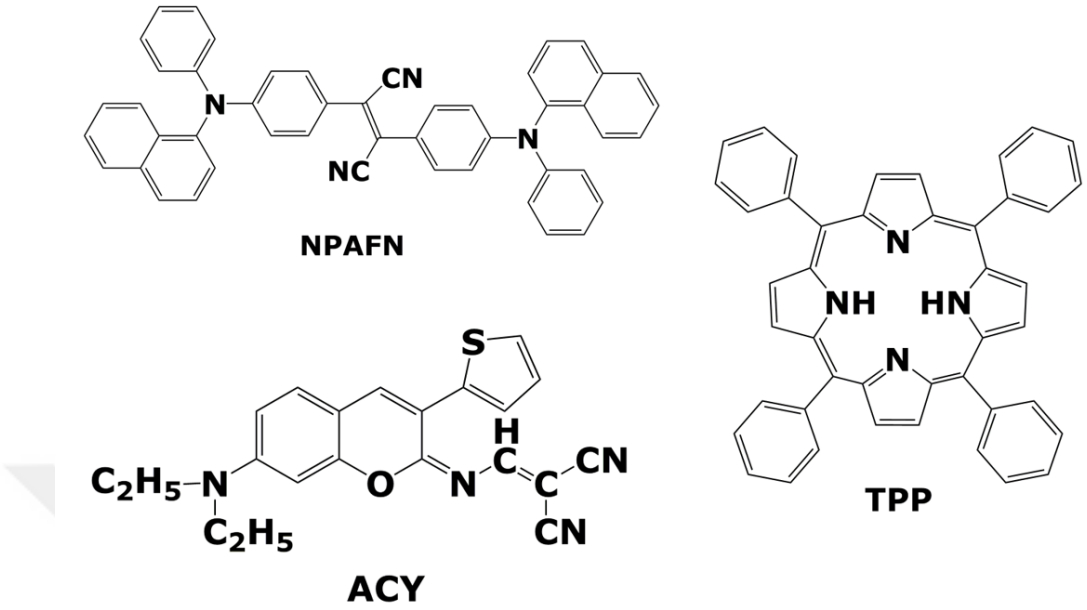

Figure 4.2. 2D structures of fluorescent (non-TADF) emitters utilized in this study.

4.2. Computational Procedure

All quantum chemistry calculations were performed using the Gaussian 09. The ground state geometries of all TADF and non-TADF emitters with their different conformations were optimized at DFT by using the M06-2X/6-31G(d) methodology in vacuum and with PCM in different solvents; cyclohexane for POZ-DBPHZ & MeODP-DBPHZ, toluene for AQ-DPA, 4CzTPN-Ph, TPA-DCPP, AQ-BBPA, AQ-DMAC, DHPZ-2BTZ, PPZ-DPS and m-Px2BBP, benzene for NPAFN, tetrahydrofuran (THF) for ACY and dichloromethane for TPP. These solvents were chosen in line with their photophysical experiments [36–46].

Singlet (S_1) and triplet excited states (T_1) of the emitters were optimized by using the same level of theory as that of the ground state. These optimizations were performed using PCM by taking into account the effects of same solvents used during ground state optimization.

Geometries optimized at ground state by M06-2X/6-31G(d) level (PCM) were taken for further calculations at their excited states (TD-DFT, TDA) with B3LYP/6-31+G(d) basis set.

Conformation analysis by changing the dihedral angles between donor and acceptor of each emitter was carried out to find the most stable and energetically favorable geometries. The most favorable conformation was chosen to report the lowest ground state and excited state energies, as well as, ΔE_{ST} values.

The accuracy of the computational method is highly required for theoretical assessments of the results, i.e., calculated values must be closer to those obtained with experimental data. Therefore, M06-2X/6-31G(d) and B3LYP/6-31+G(d) have been used.

The electron density reorganization has been analyzed in terms of NTOs obtained via the NANCY EX 2.0 software as a post process of Gaussian output and the charge transfer character has been quantified using the Φ_s index (Lowdin & Mulliken) while occupied and virtual NTOs are shown as figures to demonstrate the density overlap.

4.3. Descriptor Analysis

"Hot-exciton mechanism" occurs between upper singlet and triplet states while showing charge transfer (CT) property. In order to have high singlet production yield by strong delayed fluorescence emission and consequently by hot-exciton RISC, a 100% IQE is achieved since 75% of triplet can be converted into singlet state. The challenge of hot-exciton mechanism is to ensure higher yield of singlet states by avoiding from quenching of excitons caused by IC between T_n and T_1 states. However, typical IC rate is high in most of organic molecules with a rate of $\sim 10^{10} - 10^{9} s^{-1}$. Since it is extremely hard to compete with this rate, design of TADF emitters with an efficient RISC is a remarkably challenging task [47]. Therefore, descriptors are crucial to understand why materials demonstrate TADF character and how their efficiency can be improved. In this study, four different descriptors called twisting angle (α), low lying singlet-triplet

energy differences, ΔE_{ST}, triplet states contributed to RISC and Φ_s index with natural transition orbitals are investigated for both TADF and non-TADF emitters.

4.3.1. Twisting Angle (α)

Wang et al. showed the importance of twisting angle while generating design strategy for TADF emitters [39]. In order to have an efficient RISC process for a simple molecule, the first rule is to ensure that D and A are spatially separated with non-overlapped orbitals. This is possible by having longer spatial distance between D and A units with a molecular bridge used as a π conjugated link or increasing dihedral angle between these two units to twist around the common axis to acquire near-orthogonal structure. In each case, strong CT character should be observed in the excited states [48, 49].

Rigidification of molecule is important parameter which affects TADF efficiency. Variable conformations for a molecule may lead to different TADF yields, therefore flexibility for donor and acceptor is not favorable, especially too much change in geometry of molecules for triplet and singlet states should be avoided. Twisting of donor-acceptor bipolar structure with large dihedral angle, which it is formed as a result of bulky substitution or a spiro junction, favors RISC process for TADF molecules by contributing to the rigidity of the molecule [50]. By highly twisting the structural conformation, HOMO and LUMO are clearly separated, this is required to obtain TADF property [51]. Regarding this issue, Adachi et al. have reported that increase in dihedral angle on CZ-TRZ leads to smaller ΔE_{ST} [52].

The bond length between donor and acceptor directly affects the intramolecular charge transfer. When elongation increases, charge transfer becomes weaker by reducing the oscillator strength and consequently PLQY and EQE decreases [53]. Therefore, a balance is required while adjusting the twisting angle together with elongation of the structure for a better TADF efficiency. Twisting angles for different types of donor-acceptor designs are illustrated in Fig 4.3 [38].

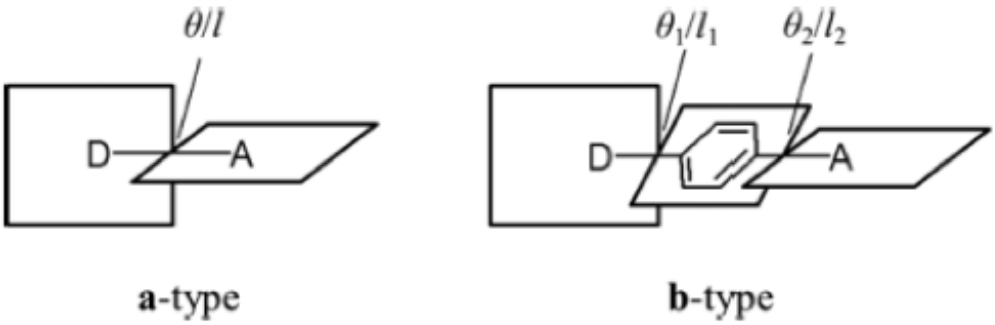

Figure 4.3. Illustration of different donor-acceptor designs

3D structures of TADF and non-TADF emitters studied in this thesis are shown in Figures 4.4 - 4.15.

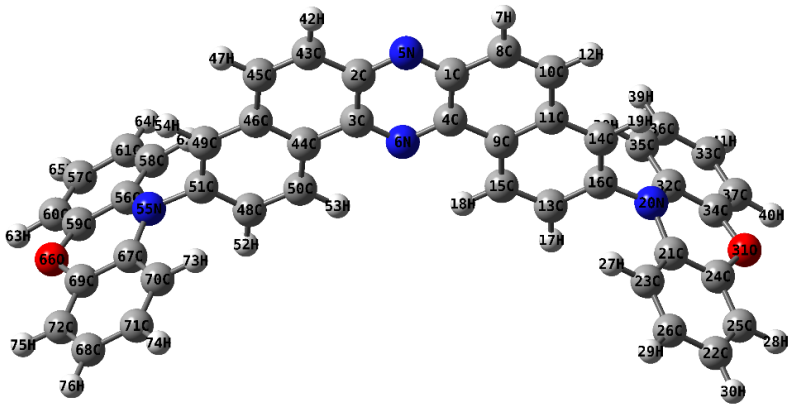

Figure 4.4. Optimized geometry of POZ-DBPHZ, red TADF emitter (M06-2X/6-31G(d)).

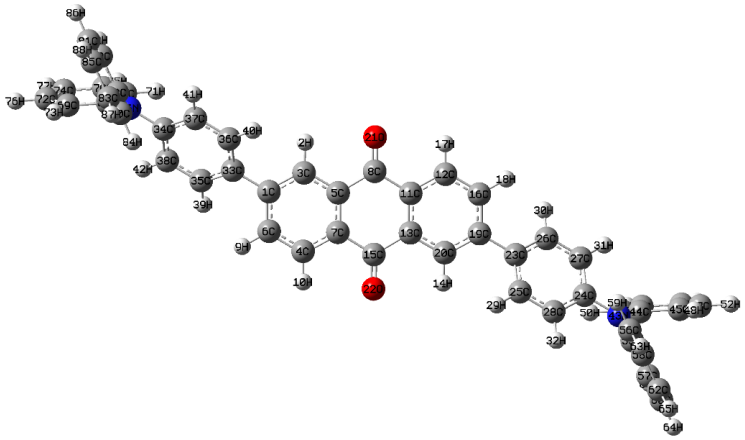

Figure 4.5. Optimized geometry of AQ-DPA, red TADF emitter (M06-2X/6-31G(d)).

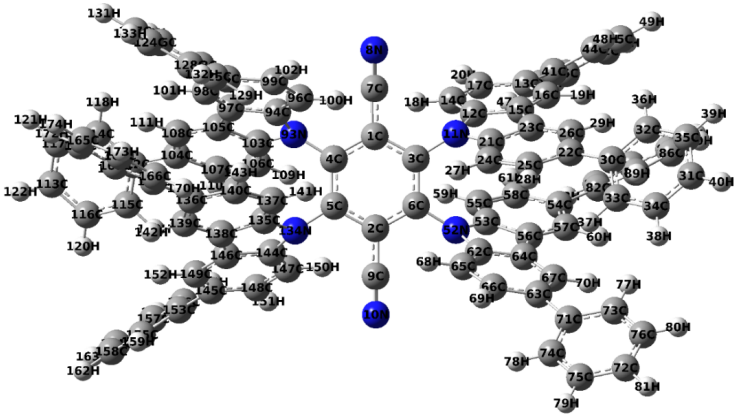

Figure 4.6. Optimized geometry of 4CzTPN-Ph, red TADF emitter (M06-2X/6-31G(d)).

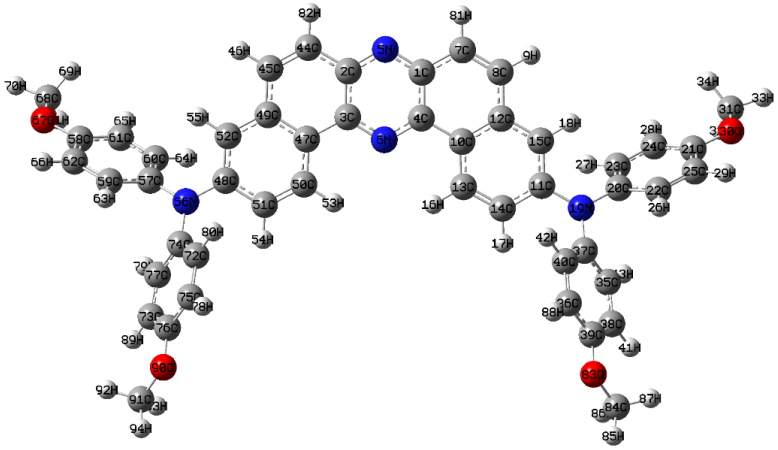

Figure 4.7. Optimized geometry of MeODP-DBPHZ, red TADF emitter (M06-2X/6-31G(d)).

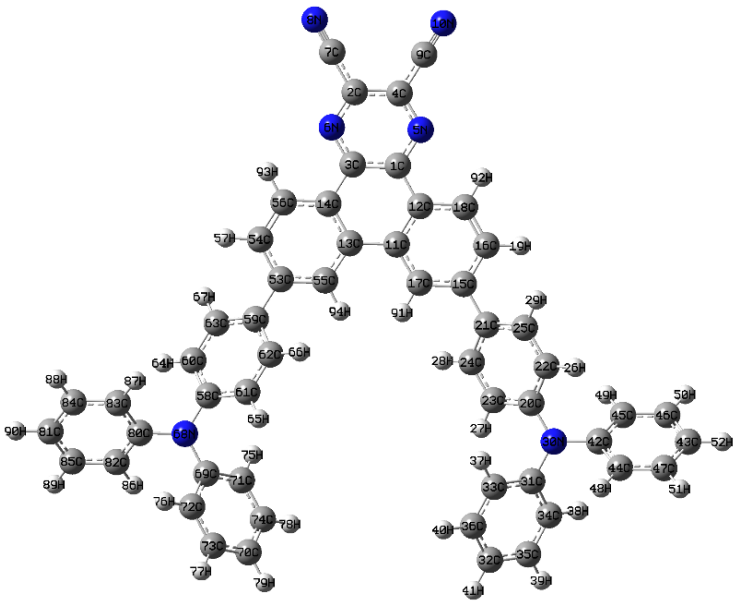

Figure 4.8. Optimized geometry of TPA-DCPP, red TADF emitter (M06-2X/6-31G(d)).

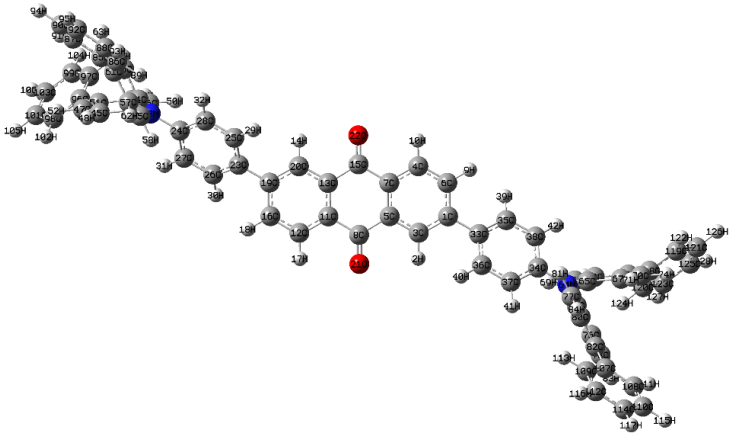

Figure 4.9. Optimized geometry of AQ-BBPA, red TADF emitter (M06-2X/6-31G(d)).

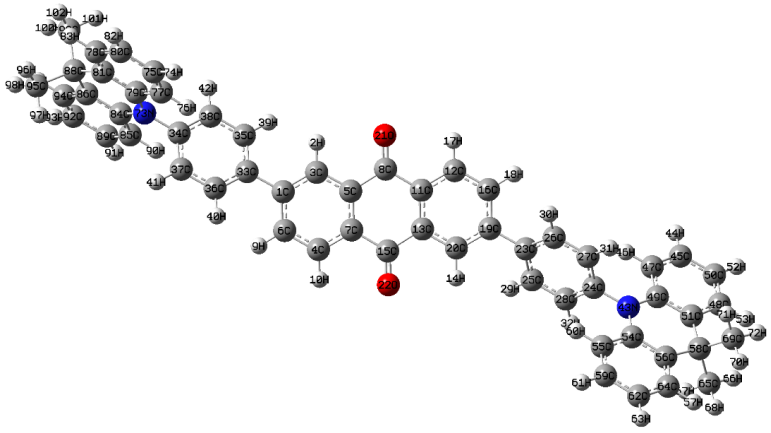

Figure 4.10. Optimized geometry of AQ-DMAC, red TADF emitter (M06-2X/6-31G(d)).

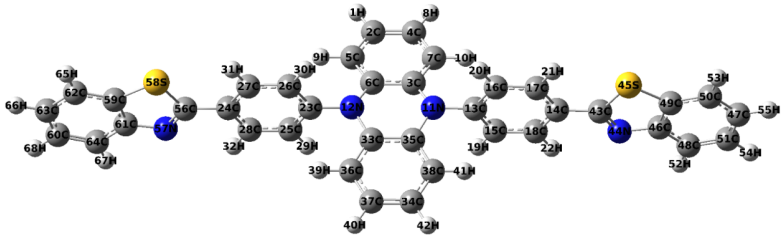

Figure 4.11. Optimized geometry of DHPZ-2BTZ, red TADF emitter (M06-2X/6-31G(d)).

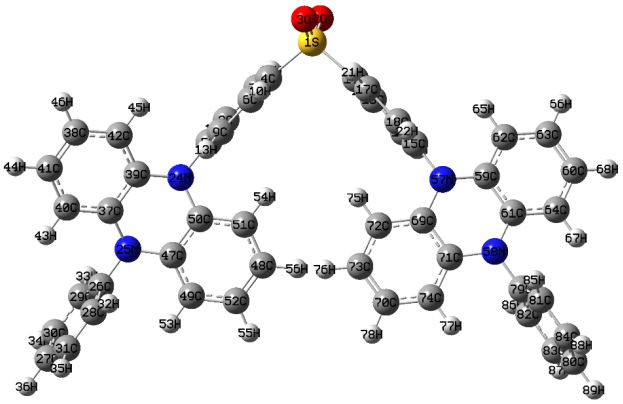

Figure 4.12. Optimized geometry of PPZ-DPS, red TADF emitter (M06-2X/6-31G(d)).

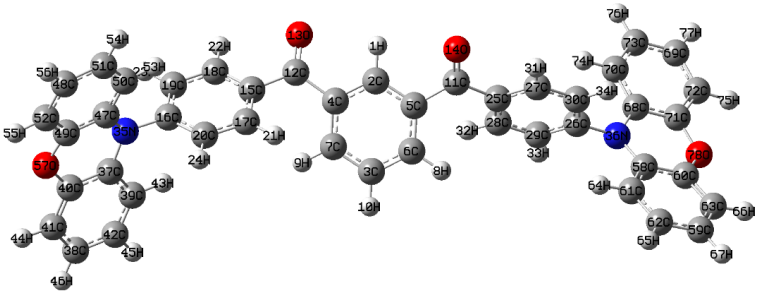

Figure 4.13. Optimized geometry of m-Px2BBP, red TADF emitter (M06-2X/6-31G(d)).

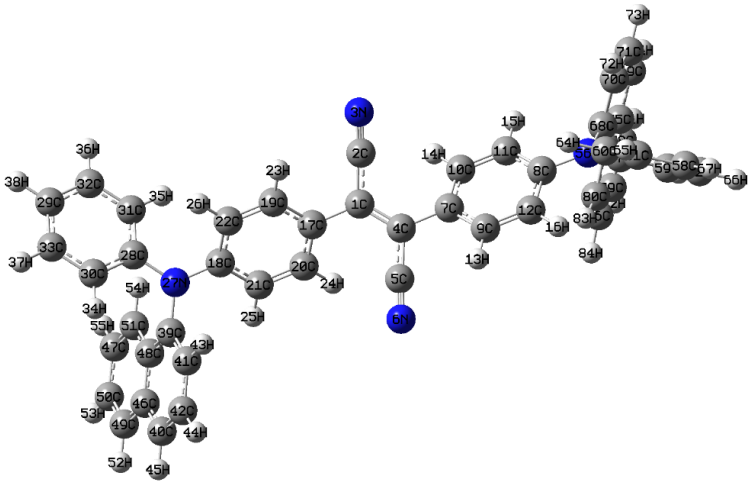

Figure 4.14. Optimized geometry of NPAFN, red non-TADF molecule (M06-2X/6-31G(d)).

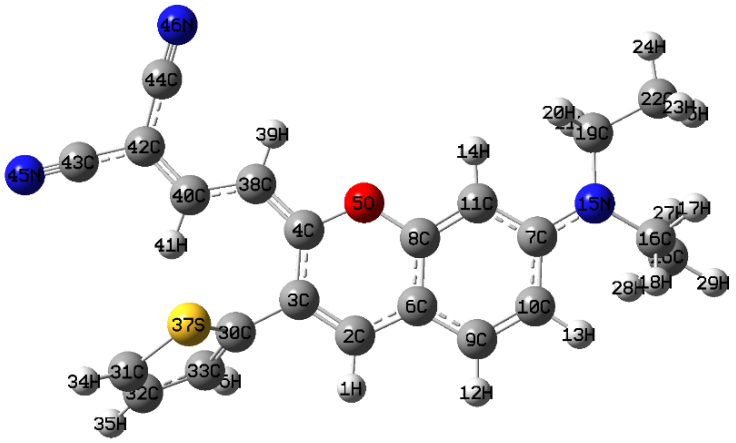

Figure 4.15. Optimized geometry of ACY, red non-TADF molecule (M06-2X/6-31G(d)).

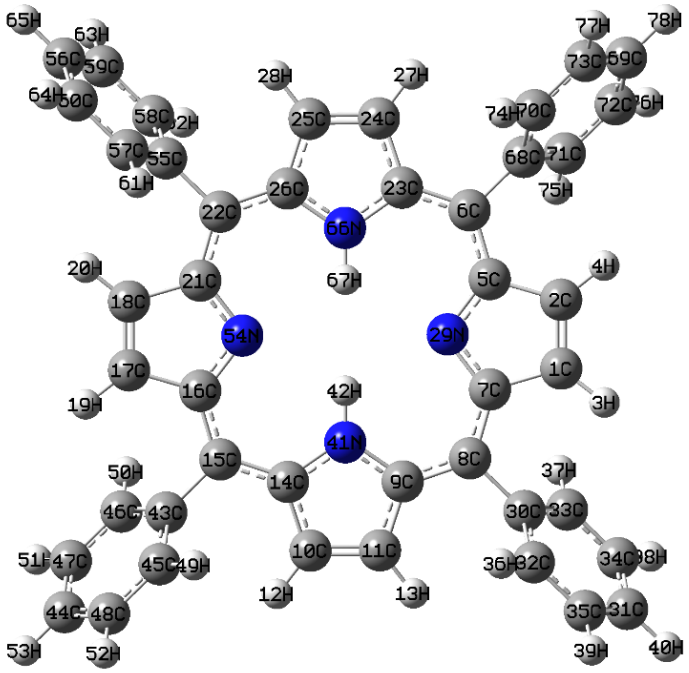

Figure 4.16. Optimized geometry of TPP, red non-TADF molecule (M06-2X/6-31G(d)).

Table 4.1. Twisting angle (α) for TADF emitters (M06-2X/6-31G(d)). X represents the phenyl bridge. (1/2)

Compound	**Design**	**Dihedral Angle**	α
POZ-DBPHZ (cyclohexane)	D-A-D	C14-C16-N20-C32	-98.81
		C49-C51-N55- C56	105.93
AQ-DPA (toluene)	D-X-A-X-D	C27-C24-N43-C55	144.44
		C16-C19-C23-C25	144.77
		C38-C34-N66-C78	144.40
		C6-C1-C33-C36	144.75
4CzTPN-Ph (toluene)	D-A-D	C94-C93-C4-C5	100.22
		C4-C5-N134-C144	99.68
		C6-C3-N11-C12	100.63
		C3-C6-N52-C62	103.41
MeODP-DBPHZ (cyclohexane)	D-A-D	C52-C48-N56-C74	-147.84
		C15-C11-N19-C37	147.88
TPA-DCPP (toluene)	D-X-A-X-D	C60-C58-N68-C69	143.54
		C54-C53-C59-C62	-147.78
		C16-C15-C21-C24	-143.45
		C22-C20-N30-C31	149.61

Table 4.2. Twisting angle (α) for TADF emitters (M06-2X/6-31G(d)). X represents the phenyl bridge. (2/2)

Compound	**Design**	**Dihedral Angle**	α
AQ-BBPA (toluene)	D-X-A-X-D	C54-N43-C24-C27	144.33
		C25-C23-C19-C16	145.34
		C6-C1-C33-C36	145.31
		C38-C34-N64-C75	144.28
AQ-DMAC (toluene)	D-X-A-X-D	C79-N73-C34-C37	87.16
		C35-C33-C1-C6	-145.74
		C16-C19-C23-C25	-144.02
		C27-C24-N43-C54	89.25
DHPZ-2BTZ (toluene)	A-D-A	C25-C23-N12-C33	-79.39
		C15-C13-N11-C35	79.39
PPZ-DPS (toluene)	D-A-D	C8-C5-N24-C50	90.94
		C19-C15-N57-C69	-85.79
m-Px2BBP (toluene)	D-A-D	C19-C16-N35-C37	102.02
		C29-C26-N36-C68	87.78

Table 4.3. Twisting angle (α) for non-TADF molecules (M06-2X/6-31G(d)).

Compound	**Design**	**Dihedral Angle**	α
NPAFN (benzene)	D-A-D	C28-N27-C18-C21	-154.09
		C11-C8-N56-C57	154.88
ACY (THF)	D-A	C4-C3-C30-C33	107.48
TPP (dichloromethane)	D-A-D	C58-C55-C22-C21	111.80
		C16-C15-C43-C45	-118.62
		C70-C68-C6-C5	117164
		C7-C8-C3C32	119.96

Twisting angle values between donor and acceptor of TADF emitters and non-TADF emitters under investigation are tabulated in Table 4.1., Table 4.2. and Table 4.3.

Twisting angles of two TADF emitters, POZ-DBPHZ and MEODP-DBPHZ, which have same acceptor units, but different donor units are compared with each other. The donor and acceptor units of POZ-DBPHZ are almost orthogonal, while MEODP-DBPHZ has around 145°, and their respective ΔE_{ST} values are 0.01 eV and 0.27 eV. This result supported that the molecular structure with twisting angle close to orthogonality has been seen to provide low ΔE_{ST} by showing better HOMO-LUMO separation.

The molecules having D-X-A-X-D design, AQ-DPA, TPA-DCPP and AQ-BBPA have bridge and show higher twisting angle around 145° deviating from orthogonality, however they have still small ΔE_{ST} values which are close to 0.1 eV (0.15 eV, 0.14 eV and 0.13 eV, respectively). It reveals that twisting angle indicating orthogonality can be considered as donor-specific descriptor for TADF emitters.

On the other hand, another emitter having the same design with the above mentioned molecules, AQ-DMAC, showed almost 90° twisting angle, even though it possesses a bridge. It is known that diphenylamine donors tend to make specifically 145° with their acceptor unit, while dimethylacridine donors in AQ-DMAC lead to orthogonality by reaching lowest ΔE_{ST} values (0.01 eV) among other structures with bridge. This revealed the importance of selecting the appropriate donors in order to have lowest ΔE_{ST} values which facilitate passing RISC barrier easily.

4.3.2. Low Lying Singlet-Triplet Energy Differences (ΔE_{ST})

The two main strategies that contribute to optimized RISC process are minimization of singlet-triplet energy gap (ΔE_{ST}) and maximization of spin-orbit coupling (SOC). Low ΔE_{ST} is achievable with a good separation of HOMO and LUMO by utilization of strong donors and acceptors. The small singlet-triplet gap initiates the

RISC process since small energy barrier makes possible easy jump of excitons. It also helps to have shorter delayed fluorescence lifetime by accelerating leap to upper state [54]. However, it is still not an easy job, other factors like molecular geometry, dielectric medium and the availability of other triplet excited states may affect the photophysical character of molecules and consequently TADF efficiency [47].

Small orbital overlap causes low ΔE_{ST} value, however, it also causes small radiative rates and so, decreased fluorescence efficiency. Besides, weak donors and acceptors play a role for small HOMO-LUMO separation, causing large singlet-triplet gap and a decreased TADF efficiency. Therefore, future investigation is required to reach a balance for structures which have small ΔE_{ST} and high fluorescence efficiency. Combining weak donors with strong acceptor in a molecule contributes to have strong TADF property with a high fluorescence yield. In such cases, different kind of weak donors are chosen for strengthening donor property of TADF emitter to reach sufficiently high fluorescence yield [47].

Uoyama et al. have claimed that ΔE_{ST} of around 0.1 eV is ideal for TADF [55]. Besides, Dias et al. have shown by detailed spectroscopic measurements on a range of TADF materials, that even with such large ΔE_{ST} which is above 0.3 eV, 100% TADF efficiency is still achievable [56]. When ΔE_{ST} are less than 0.4 eV and the SOC between singlet and triplet excited states are similar for small organic molecules, a decrease of an order of magnitude in ΔE_{ST} causes an increase of several orders of magnitude in RISC rate [57].

Table 4.4. Low lying singlet-triplet energy differences, ΔE_{ST} (eV), for TADF emitters (B3LYP/6-31+G(d) by TD-DFT and TDA) together with their experimental values.

Compound	**TD-DFT**	**TDA**	**Experimental**
POZ-DBPHZ (cyclohexane)	0.01	0.01	0.02
AQ-DPA (toluene)	0.15	0.15	0.24
4CzTPN-Ph (toluene)	0.09	0.09	-
MeODP-DBPHZ (cyclohexane)	0.27	0.27	0.19
TPA-DCPP (toluene)	0.15	0.14	0.13
AQ-BBPA (toluene)	0.13	0.13	0.22
AQ-DMAC (toluene)	0.01	0.01	0.07
DHPZ-2BTZ (toluene)	0.01	0.01	0
PPZ-DPS (toluene)	0.01	0.01	0.08
m-Px2BBP (toluene)	0.03	0.03	0.10

Table 4.5. Low lying singlet-triplet energy differences, ΔE_{ST} (eV), for non-TADF molecules (B3LYP/6-31+G(d) by TD-DFT and TDA).

Compound	**TD-DFT**	**TDA**
NPAFN (benzene)	0.54	0.43
ACY (THF)	0.86	0.91
TPP (dichloromethane)	0.73	0.56

All values for low-lying singlet-triplet energy difference are tabulated in Table 4.4. and 4.5.

It has been clearly shown that all TADF emitters investigated in this study have smaller singlet-triplet values, below 0.3 eV. Most of them showed values close or below 0.1 eV, while non-TADF emitters have higher singlet-triplet value than 0.5 eV.

4.3.3. Triplet States Contribution to RISC

Huang et al. reported that ΔE_{S1-T1} gap is not the most significant parameter, instead, ΔE_{T1-Tn} energy gap should also be considered when degenerate or close excited states are available. When T_2 state is much closer to S_1 state than T_1 in energy, then it can be defined as another RISC pathway from T_2 to S_1. According to Kasha's rule, this kind of approach helps to have efficient internal conversion among triplet states and vertical route for emission of initially associated triplet to the lowest state [58]. This is clearly illustrated by Jablonski diagram in Fig 4.17 [59].

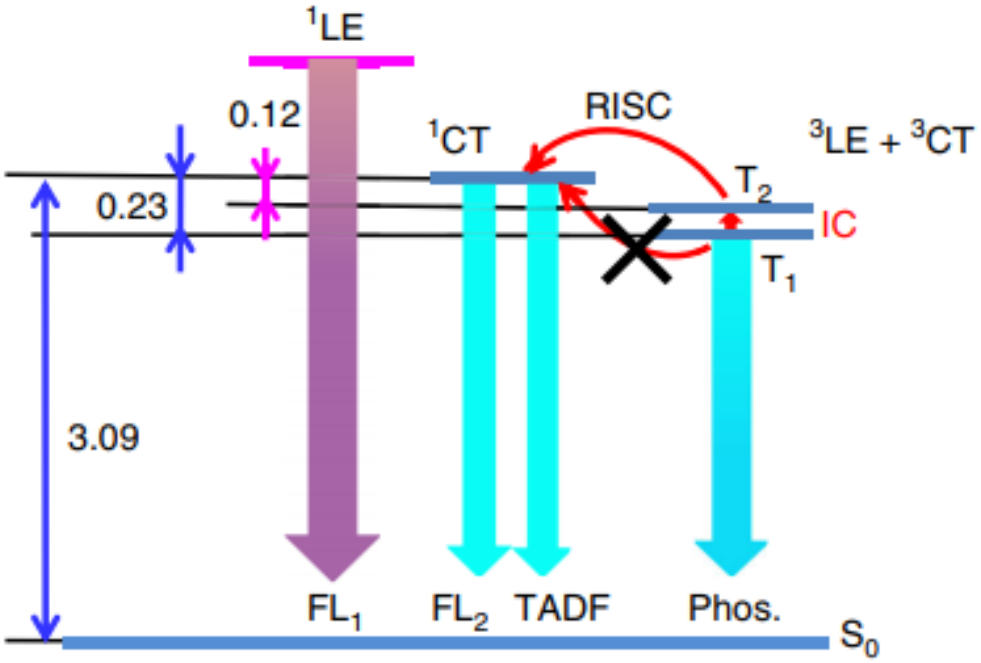

Figure 4.17. Jablonski diagram for a proposed emissive mechanism with alternative RISC pathway

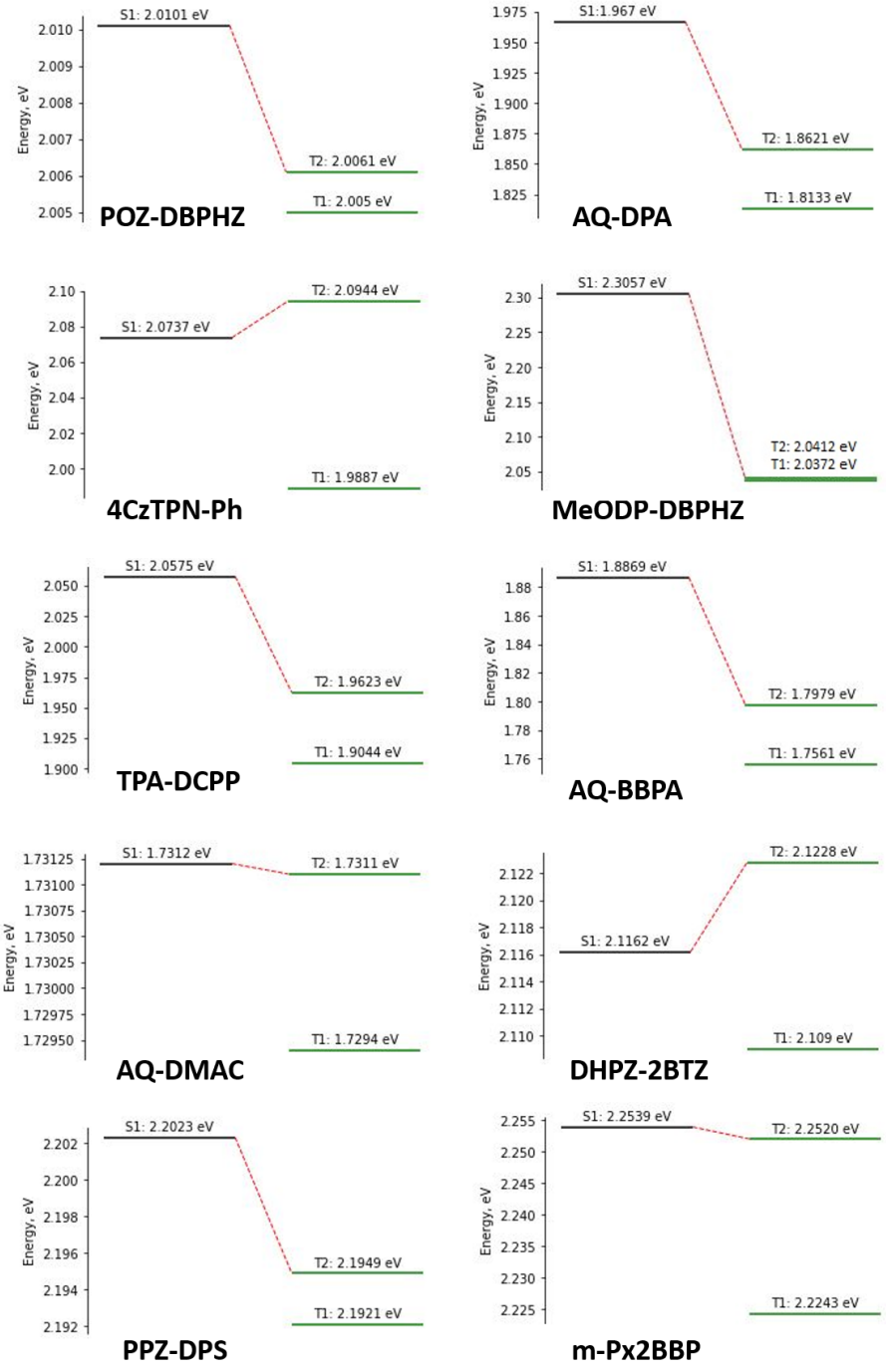

Figure 4.18. Schematic diagram showing triplet states closest to S_1 for TADF emitters.

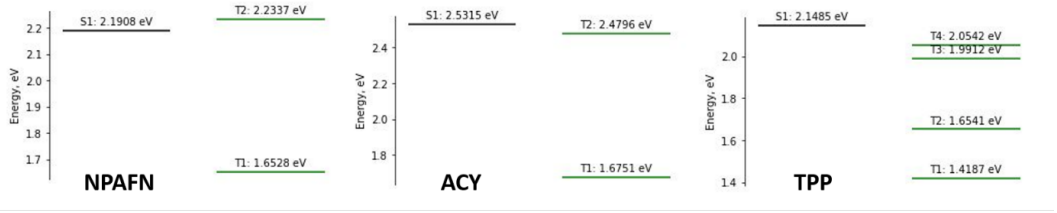

Figure 4.19. Schematic diagram showing triplet states closest to S_1 for non-TADF emitters.

Table 4.6. Energy difference in closest singlet-triplet states, ΔE_{S1-T2} (eV), low lying singlet-triplet energy differences, ΔE_{S1-T1} (eV) and energy difference in relevant triplet states, ΔE_{T1-T2} (eV), contributing to RISC of TADF emitters (B3LYP/6-31+G(d) by TD-DFT).

Compound	**RISC Nature**	ΔE_{T1-T2}	ΔE_{S1-T2}	ΔE_{S1-T1}
POZ-DBPHZ (cyclohexane)	$T_2 \rightarrow S_1$	0.0011	0.0040	0.0051
AQ-DPA (toluene)	$T_2 \rightarrow S_1$	0.0488	0.1049	0.1537
4CzTPN-Ph (toluene)	$T_2 \rightarrow S_1*$	0.1057	0.0207	0.0850
MeODP-DBPHZ (cyclohexane)	$T_2 \rightarrow S_1$	0.0040	0.2645	0.2685
TPA-DCPP (toluene)	$T_2 \rightarrow S_1$	0.0579	0.0952	0.1531
AQ-BBPA (toluene)	$T_2 \rightarrow S_1$	0.0418	0.0890	0.1308
AQ-DMAC (toluene)	$T_2 \rightarrow S_1$	0.0017	0.0001	0.0018
DHPZ-2BTZ (toluene)	$T_2 \rightarrow S_1*$	0.0138	0.0066	0.0072
PPZ-DPS (toluene)	$T_2 \rightarrow S_1$	0.0028	0.0074	0.0102
m-Px2BBP (toluene)	$T_2 \rightarrow S_1$	0.0277	0.0019	0.0296

* represents RISC from T_2 which is higher in energy than S_1.

Table 4.7. Energy difference in closest singlet-triplet states, ΔE_{S1-T2} (eV), low lying singlet-triplet energy differences, ΔE_{S1-T2} (eV) and energy difference in relevant triplet states, ΔE_{T1-T*} (eV) (B3LYP/6-31+G(d) by TD-DFT).

Compound	ΔE_{T1-T*}	ΔE_{S1-T2}	ΔE_{S1-T1}
NPAFN (benzene)	0.5809	0.0429	0.5380
ACY (THF)	0.8045	0.0519	0.8564
TPP (dichloromethane)	0.6355	0.0947	0.7298

* represents the closest triplet state to singlet state; T_2 for NPAFN and ACY, T4 for TPP.

Energy differences in closest singlet-triplet states, ΔE_{S1-T2} (eV), with energy difference in relevant triplet states, ΔE_{T1-T2} (eV), contributing to RISC for TADF and non-TADF emitters used in this study are shown in Table 4.6. and 4.7.

Schematic diagram in Fig 4.18. shows that TADF emitters in this study have two triplet states which are lower in energy than S_1. In light of this, alternative RISC is possible by contribution of T_2 to S_1 state. Only two of TADF emitters have T_2 states which are higher in energy than S_1. Different design strategies can be the reason of it since DHPZ-2BTZ is the only molecule having A-D-A structure and 4CzTPN-Ph has 4 donors around acceptor while others have 2 donors within D-A-D structure.

Schematic diagram in Fig 4.19. demonstrates that some non-TADF emitters have triplet states lower in energy than S_1, however since their low-lying singlet-triplet energies are higher than 0.3 eV, they cannot be considered as TADF emitter. This reveals that this descriptor should be considered together with other descriptors utilized

in this study while guessing TADF activity of an emitter.

4.3.4. Φ_s Index & Natural Transition Orbitals

Φ_s index is based on the normalized overlap of the detachment and attachment density matrix, therefore values close to 1.0 describe a local excitation, while values close to 0 show a significant charge-transfer [60].

Table 4.8. Φ_s indices for TADF emitters in Lowdin (L) and Mulliken (M) charge distributions (B3LYP/6-31+G(d) by TD-DFT and TDA).

Compound	Transition	TD-DFT		TDA	
		L	M	L	M
POZ-DBPHZ (cyclohexane)	$S_0 \rightarrow S_1$	0.0793	0.1219	0.0767	0.1195
AQ-DPA (toluene)	$S_0 \rightarrow S_1$	0.3827	0.4156	0.3386	0.3854
4CzTPN-Ph (toluene)	$S_0 \rightarrow S_1$	0.3111	0.3836	0.3255	0.3961
MeODP-DBPHZ (cyclohexane)	$S_0 \rightarrow S_1$	0.5729	0.6250	0.5989	0.6506
TPA-DCPP (toluene)	$S_0 \rightarrow S_1$	0.3003	0.3244	0.3409	0.3633
AQ-BBPA (toluene)	$S_0 \rightarrow S_1$	0.3002	0.3301	0.3053	0.3348
AQ-DMAC (toluene)	$S_0 \rightarrow S_1$	0.1542	0.1825	0.1366	0.1650
DHPZ-2BTZ (toluene)	$S_0 \rightarrow S_1$	0.0543	0.1444	0.0374	0.1251
PPZ-DPS (toluene)	$S_0 \rightarrow S_1$	0.2236	0.4549	0.1301	0.2877
m-Px2BBP (toluene)	$S_0 \rightarrow S_1$	0.2234	0.3161	0.2222	0.3118

Table 4.9. Φ_s indices for non-TADF molecules in Lowdin (L) and Mulliken (M) charge distributions (B3LYP/6-31+G(d) by TD-DFT and TDA).

Compound	Transition	TD-DFT		TDA	
		L	M	L	M
NPAFN (benzene)	$S_0 \rightarrow S_1$	0.5834	0.6222	0.6005	0.6405
ACY (THF)	$S_0 \rightarrow S_1$	0.6315	0.6593	0.6297	0.6596
TPP (dichloromethane)	$S_0 \rightarrow S_1$	0.9513	1.0557	0.9649	1.0736

Φ_s index values for both TADF emitters and non-TADF emitters under investigation are found in Table 4.8. and 4.9.

All TADF emitters except for MeODP-DBPHZ show small indices close to 0, while non-TADF emitters resulted in higher indices, showing high overlap between occupied and virtual orbitals.

Table 4.10. Occupied and virtual NTO's for the TADF emitters (B3LYP/6-31+G(d)) (1/3).

Compound	**Occupied**	**Virtual**
POZ-DBPHZ (cyclohexane)	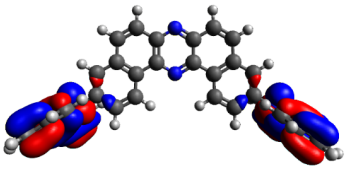	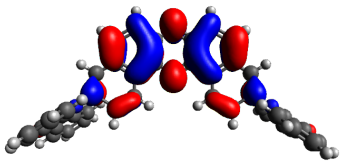
AQ-DPA (toluene)	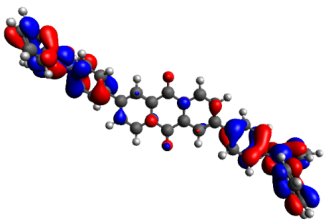	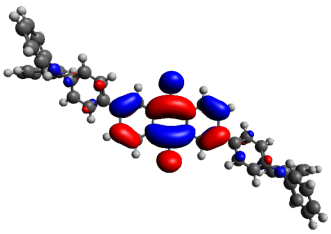
4CzTPN-Ph (toluene)	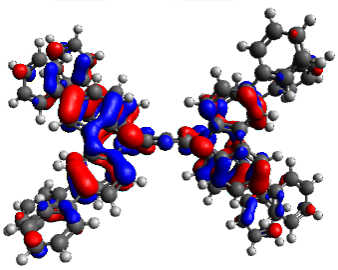	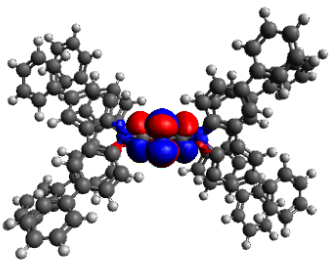

Table 4.11. Occupied and virtual NTO's for the TADF emitters (B3LYP/6-31+G(d)) (2/3).

Compound	**Occupied**	**Virtual**
MeODP-DBPHZ (cyclohexane)	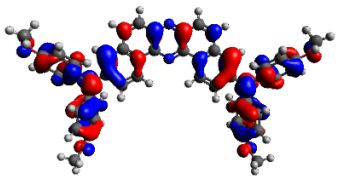	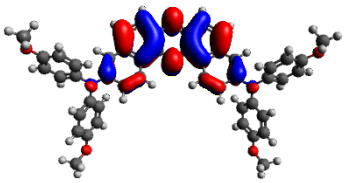
TPA-DCPP (cyclohexane)	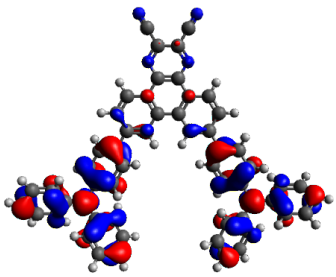	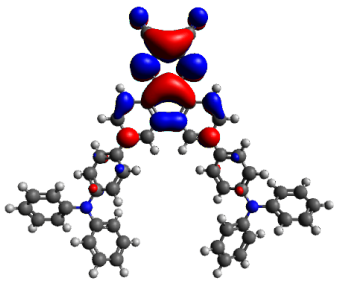
AQ-BBPA (cyclohexane)	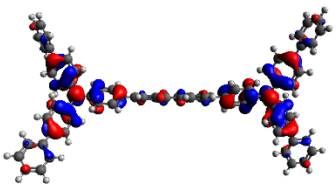	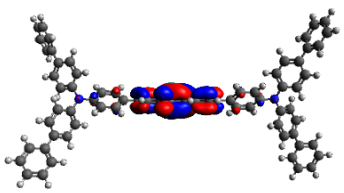

Table 4.12. Occupied and virtual NTO's for the TADF emitters (B3LYP/6-31+G(d)) (3/3).

Compound	**Occupied**	**Virtual**
AQ-DMAC (toluene)	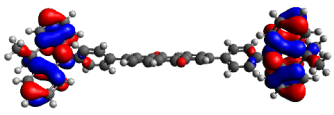	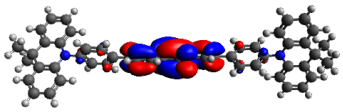
DHPZ-2BTZ (toluene)	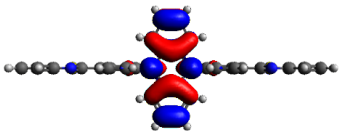	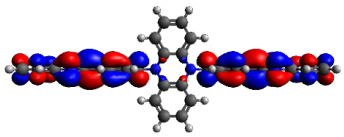
PPZ-DPS (toluene)	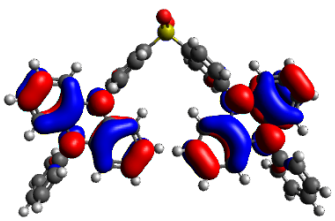	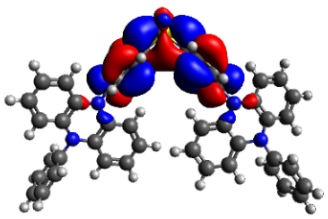
m-Px2BBP (toluene)	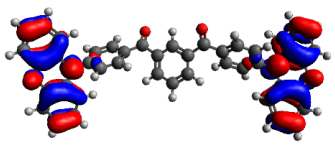	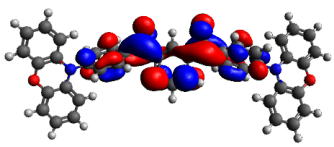

Table 4.13. Occupied and virtual NTO's for the non-TADF emitters (B3LYP/6-31+G(d)).

Compound	**Occupied**	**Virtual**
NPAFN (benzene)	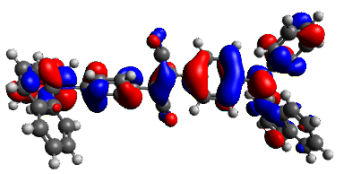	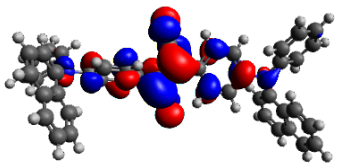
ACY (THF)	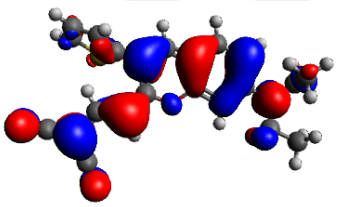	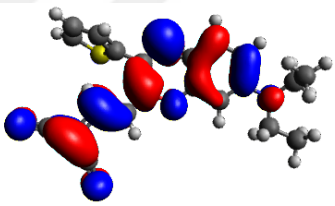
TPP (dichloromethane)	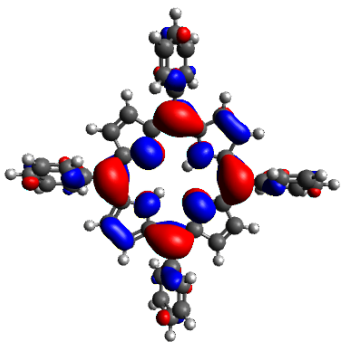	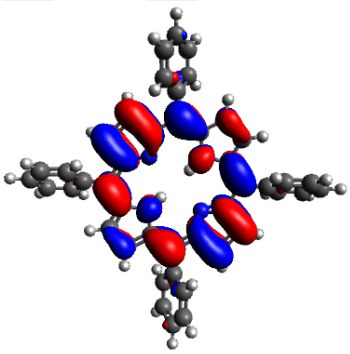

5. CONCLUSION

The computational study for ten red TADF OLED emitters which have different donor and acceptors in various molecular design structures, was conducted to understand the relationship between molecular structures and their photophysical properties. In addition, three red fluorescent (non-TADF) emitters were utilized as cross comparison group to understand TADF mechanism in detail for being able to suggest potential TADF molecular structures and accelerate the design development of TADF OLEDs. Conformation analysis was carried out by changing the dihedral angles between donor and acceptor of each emitter in order to find the most stable geometries. For each molecule, the lowest energy conformation was chosen to tabulate the ground state and excited state energies, as well as, ΔE_{ST} values.

In this study, it has been shown that the emitters should meet the criteria for four identified descriptors (twisting angle, low lying singlet triplet energy difference, triplet states contributing to RISC and Φ_s index with NTOs) to have TADF property for OLEDs. The descriptors have revealed that molecular structures with twisting angle close to orthogonal values provide lower ΔE_{ST} value by having better HOMO-LUMO separation. Although adding bridge between donor and acceptor increases the twisting angle, it helps the delocalization of electrons within longer structure to have still small ΔE_{ST} value which is close to 0.1 eV. In addition, it has been clearly shown that all TADF emitters have smaller ΔE_{ST} values, below 0.3 eV, while non-TADF emitters have higher ΔE_{ST} value than 0.5 eV. All TADF emitters, except MeODP-DBPHZ have shown smaller Φ_s indices which are close to 0, while non-TADF emitters have higher Φ_s indices, indicating high overlap between occupied and virtual orbitals. TADF emitters have two triplet states which are lower in energy than S_1. In light of this, alternative RISC is possible by the contribution of T_2 to S_1 state. Only two of TADF emitters have T_2 states which are higher in energy than S_1, however, since the energy difference between T_1 to T_2 together with T_2 to S_1 are still low, around 0.1 eV, alternative RISC can also be considered for them.

TADF emitters are well separated from non-TADF emitters by four descriptors utilized in this study. These descriptors reveal that they can be further used while developing a design strategy including the modification of already known molecular structures of emitters or predicting novel TADF emitters to be efficient in OLEDs.

6. FUTURE REMARKS

At present, there are several characterization techniques to find out TADF properties, however more solid actions are necessary to understand overall concept for being able to commercialize OLEDs. The fabrication costs are significantly high for TADF OLEDs utilized in display and lightening industries. Therefore, solution-based OLEDs and polymeric or dendrimeric TADF emitters should be developed to reduce the cost. These kind of TADFs have important role in next generation displays and lightning materials and they will find broad usage when their synthesis characterization and device manufacturing processes are clearly identified [48].

Easy crystallization of small-molecule TADF emitters causes poor solubility and they are stored by thermal evaporation at high temperature in vacuum, thus small sized OLED devices can be produced at high cost. On the other hand, several solution techniques such as spin-coating, ink-jetting and flow casting provide easy processability to electroluminescent polymers while preparing them, thus large-scale fabrication for polymeric fluorescent OLEDs has high potential since its first report by Friend et al. in 1990. Despite transferable characteristic of small TADF molecules to polymers, only few studies on TADF polymer emitters are available for now [61].

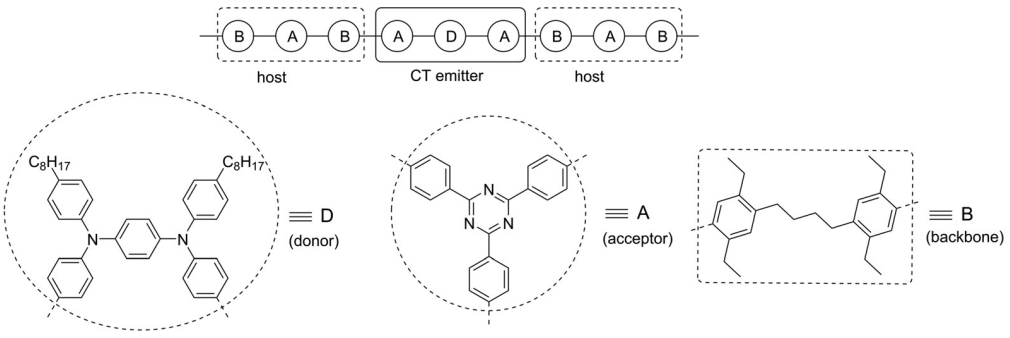

Figure 6.1. Chemical structures of a TADF polymer

OLED devices with small molecule emitters which show phosphorescent or TADF properties reach external quantum efficiencies above 25% when doped into an appropriate host. Simple device fabrication can be achieved by omitting the host materials. Host-free devices which have thin film of emitter in emission layer, demonstrate generally poor roll-off in efficiency due to aggregation such as luminescence quenching and spectral shift. Polymers or dendrimers called self-host materials show both emitter and host structural properties and they are accepted as alternative to host-free devices [62].

As a future work, several donor and acceptor units found in a polymer or dendrimer will be computationally analyzed by using the descriptors utilized in this study. By this way, possible TADF polymers or dendrimers can be suggested in order to be used in a host-free OLED devices.

REFERENCES

1. Frangopoulos, C. A., "Recent developments and trends in optimization of energy systems", *Energy*, Vol. 164, pp. 1011–1020, 2018.

2. Uribe-Toril, J., J. L. Ruiz-Real, J. Milán-García and J. P. Valenciano, "Energy, Economy, and Environment: A Worldwide Research Update", *Energies*, Vol. 12, p. 1120, 2019.

3. Dincer, I., "Renewable energy and sustainable development: a crucial review", *Renewable and Sustainable Energy Reviews*, Vol. 4, pp. 157–175, 2000.

4. Moriarty, P. and D. Honnery, "What is the global potential for renewable energy?", *Renewable and Sustainable Energy Reviews*, Vol. 16, p. 244–252, 2012.

5. Oliveira, C. and C. H. Antunes, "A multiple objective model to deal with economy–energy–environment interactions", *European Journal of Operational Research*, Vol. 153, p. 370–385, 2004.

6. Kahouli-Brahmi, S., "Technological learning in energy–environment–economy modelling: A survey", *Energy Policy*, Vol. 36, p. 138–162, 2008.

7. Hanley, N., P. G. McGregor, J. K. Swales and K. Turner, "Do increases in energy efficiency improve environmental quality and sustainability?", *Ecological Economics*, Vol. 68, p. 692 – 709, 2009.

8. Chen, H., J. Lee, B. Lin, S. Chen and S. Wu, "Liquid crystal display and organic light-emitting diode display: present status and future perspectives", *Light: Science & Applications*, Vol. 7, p. 17168, 2018.

9. Kobayashi, T., H. Kanematsu, R. Hashimoto, K.Morisato, N. Ohashi, H. Yamasaki and S. Takamiya, "Study on environment and energy using belonging materials",

International Journal of Sustainable Development & World Policy, Vol. 2(4), pp. 50–58, 2013.

10. Patel, B. N. and M. M. Prajapati, "OLED: A Modern Display Technology", *International Journal of Scientific and Research Publications*, Vol. 4, 2014.

11. Aizawa, N., I. S. Park and T. Yasuda, "Design of Thermally Activated Delayed Fluorescence Materials for Organic Light-Emitting Diodes", *AAPPS BULLETIN*, Vol. 26, 2016.

12. Chatterjee, T. and K. Wong, "Perspective on Host Materials for Thermally Activated Delayed Fluorescence Organic Light Emitting Diodes", *Adv. Optical Mater.*, Vol. 7, p. 1800565, 2019.

13. Wong, M. Y. and E. Zysman-Colman, "Purely Organic Thermally Activated Delayed Fluorescence Materials for Organic Light-Emitting Diodes", *Adv. Mater.*, Vol. 29, p. 1605444, 2017.

14. Jung, M., K. H. Lee, W. P. Hong and J. Y. Lee, "Effect of frontier orbital distribution of the core structure on the photophysics and device performances of thermally activated delayed fluorescent emitters", *Journal of Materials Chemistry C*, Vol. 7, pp. 7760–7767, 2019.

15. Aydemir, M., S. Xu, C. Chen, M. R. Bryce, Z. Chi and A. P. Monkman, "Photophysics of an Asymmetric Donor−Acceptor−Donor′ TADF Molecule and Reinterpretation of Aggregation-Induced TADF Emission in These Materials", *J. Phys. Chem. C*, Vol. 121, p. 17764−17772, 2017.

16. Rajamalli, P., D. Chen, W. Li, I. D. W. Samuel, D. B. Cordes, A. M. Z. Slawin and E. Zysman-Colman, "Enhanced Thermally Activated Delayed Fluorescence Through Bridge Modification in Sulfone-Based Emitters Employed in Deep Blue Organic Light-Emitting Diodes", *J. Mater. Chem. C*, Vol. 7, pp. 6664–6671, 2019.

17. Im, Y., M. Kim, Y. J. Cho, J. Seo and K. S. Yook, "Molecular Design Strategy of Organic Thermally Activated Delayed Fluorescence Emitters", *Chem. Mater.*, Vol. 29, p. 1946−1963, 2017,.

18. Zhang, S., L. Yao, Q. Peng, W. Li, Y. Pan, R. Xiao, Y. Gao, C. Gu, Z. Wang, P. Lu, F. Li, S. Su, B. Yang and Y. Ma, "Achieving a Significantly Increased Efficiency in Nondoped Pure Blue Fluorescent OLED: A Quasi-Equivalent Hybridized Excited State", *Adv. Funct. Mater.*, Vol. 25, p. 1755–1762, 2015.

19. Penfold, T. J., F. B. Dias and A. P. Monkman, "The theory of thermally activated delayed fluorescence for organic light emitting diodes", *Chem. Commun.*, Vol. 54, pp. 3926–3935, 2018.

20. Chen, J., K. Wang, C. Zheng, M. Zhang, Y. Shi, S. Tao, H. Lin, W. Liu, W. Tao, X. Ou and X. Zhang, "Red Organic Light-Emitting Diode with External Quantum Efficiency beyond 20% Based on a Novel Thermally Activated Delayed Fluorescence Emitter", *Adv. Sci.*, Vol. 5, p. 1800436, 2018.

21. Tsuneda, T., *Density Functional Theory in Quantum Chemistry*, Springer, Japan, 2014.

22. Leach, A. R., *Molecular Modelling, Principles and Applications*, Pearson Education Limited, England, 2001.

23. Wills, J. M., M. Alouani, P. Andersson, A. Delin, O. Eriksson and O. Grechnyev, *Full-Potential Electronic Structure Method*, Springer, Germany, 2010.

24. Adamo, C. and D. Jacquemin, "The calculations of excited-state properties with Time-Dependent Density Functional Theory", *Chem. Soc. Rev.*, Vol. 42, pp. 845–856, 2013.

25. Marques, M. A. L., C. A. Ullrich, F. Nogueira, A. Rubio, K. Burke and E. K. U. Gross, *Time-Dependent Density Functional Theory*, Springer, Germany, 2006.

26. Cheng, C. Y., M. S. Ryley, M. J. Peach, D. J. Tozer, T. Helgaker and A. M. Teale, "Molecular properties in the Tamm–Dancoff approximation: indirect nuclear spin–spin coupling constants", *Molecular Physics*, Vol. 113, pp. 1937–1951, 2015.

27. Sander, T., E. Maggio and G. Kresse, "Beyond the Tamm-Dancoff approximation for extended systems using exact diagonalization", *Physcial Review B*, Vol. 92, p. 045209, 2015.

28. Schuchardt, K. L., B. T. Didier, T. Elsethagen, L. Sun and V. Gurumoorthi, "Basis Set Exchange: A Community Database for Computational Sciences", *J. Chem. Inf. Model.*, Vol. 47, pp. 1045–1052, 2007.

29. Ramachandran, K. I., G. Deepa and K. Namboori, *Computational Chemistry and Molecular Modeling*, Springer, Germany, 2008.

30. McQuarrie, D. A. and J. D. Simon, *Physical Chemistry, A Molecular Approach*, University of Science Books, USA, 1997.

31. Klamt, A. and V. Jonas, "Treatment of the outlying charge in continuum solvation models", *J. Chem. Phys.*, Vol. 105, p. 9972, 1996.

32. Im, W., D. Beglov and B. Roux, "Continuum Solvation Model: computation of electrostatic forces from numerical solutions to the Poisson-Boltzmann equation", *Computer Physics Communications*, Vol. 111, pp. 59–75, 1998.

33. Etienne, T., "Theoretical Insights into the Topology of Molecular Excitons from Single-Reference Excited States Calculation Methods", *Intech Open*, Vol. Chapter 3, pp. 31–54, 2017.

34. Endo, A., K. Sato, K. Yoshimura, T. Kai, A. Kawada, H. Miyazaki and C. Adachi, "Efficient up-conversion of triplet excitons into a singlet state and its application for organic light emitting diodes", *Appl. Phys. Lett.*, Vol. 98, p. 083302, 2011.

35. Kumar, M., M. Ribeiro and L. Pereira, "New Generation of High Efficient OLED Using Thermally Activated Delayed Fluorescent Materials", *Intech Open*, Vol. Chapter 6, pp. 103–126, 2018.

36. Data, P., P. Pander, M. Okazaki, Y. Takeda, S. Minakata and A. P. Monkman, "Dibenzo[a,j]phenazine-Cored Donor–Acceptor–Donor Compounds as Green-to-Red/NIR Thermally Activated Delayed Fluorescence Organic Light Emitters", *Angew. Chem. Int. Ed.*, Vol. 55, pp. 5739–5744, 2016.

37. Zhang, Q., H. Kuwabara, W. J. Potscavage, S. Huang, Y. Hatae, T. Shibata and C. Adachi, "Anthraquinone-Based Intramolecular Charge-Transfer Compounds: Computational Molecular Design, Thermally Activated Delayed Fluorescence, and Highly Efficient Red Electroluminescence", *J. Am. Chem. Soc.*, Vol. 136, pp. 18070–18081, 2014.

38. Uoyama, H., K. Goushi, K. Shizu, H. Nomura and C. Adachi, "Highly efficient organic light-emitting diodes from delayed fluorescence", *Nature*, Vol. 492, pp. 234–240, 2012.

39. Wang, S., X. Yan, Z. Cheng, H. Zhang, Y. Liu and Y. Wang, "Highly Efficient Near-Infrared Delayed Fluorescence Organic Light Emitting Diodes Using a Phenanthrene-Based Charge-Transfer Compound", *Angew. Chem. Int. Ed.*, Vol. 54, pp. 13068–13072, 2015.

40. Lee, J., K. Shizu, H. Tanaka, H. Nakanotani, T. Yasuda, H. Kaji and C. Adachi, "Controlled emission colors and singlet–triplet energy gaps of dihydrophenazine-based thermally activated delayed fluorescence emitters", *J. Mater. Chem. C.*, Vol. 3, pp. 2175–2181, 2015.

41. Zhang, Q., B. Li, S. Huang, H. Nomura, H. Tanaka and C. Adachi, "Efficient blue organic light-emitting diodes employing thermally activated delayed fluorescence", *Nature Photonics*, Vol. 8, pp. 326–332, 2014.

42. Lee, S. Y., T. Yasuda, Y. S. Yang, Q. Zhang and C. Adachi, "Luminous Butterflies: Efficient Exciton Harvesting by Benzophenone Derivatives for Full-Color Delayed Fluorescence OLEDs", *Angew. Chem*, Vol. 126, pp. 6520–6524, 2014.

43. Chen, C., "Evolution of Red Organic Light-Emitting Diodes: Materials and Devices", *Chem. Mater*, Vol. 16, pp. 4389–4400, 2004.

44. Yeh, H., S. Yeh and C. Chen, "Readily synthesised arylamino fumaronitrile for non-doped red organic light-emitting diodes", *Chem. Commun.*, Vol. 20, pp. 2632–2633, 2003.

45. Yu, J. and Y. Shirota, "A New Class of High-Performance Red-Fluorescent Dyes for Organic Electroluminescent Devices", *Chem. Lett.*, Vol. 105, pp. 984–985, 2002.

46. Burrows, P. and S. R. Forrest, "Color-Tunable Organic Light Emitting Devices", *Appl. Phys. Lett*, Vol. 69, pp. 82–83, 1996.

47. Dias, F., T. Penfold and A. Monkman, "Photophysics of thermally activated delayed fluorescence molecules", *Methods Appl. Fluoresc.*, Vol. 5, p. 012001, 2017.

48. Kukhta, N. A., H. F. Higginbotham, T. Matulaitis, A. Danos, A. N. Bismillah, N. Haase, M. K. Etherington, D. S. Yufit, P. R. McGonigal, J. V. Grazulevicius and A. P. Monkman, "Revealing resonance effects and intramolecular dipole interactions in the positional isomers of benzonitrile-core thermally activated delayed fluorescence materials", *J. Mater. Chem. C*, Vol. 7, pp. 9184–9194, 2019.

49. Silva, P., C. A. Kim, T. Zhu and T. V. Voorhis, "Extracting Design Principles for Efficient Thermally Activated Delayed Fluorescence (TADF) from a Simple Four-State Model", *ChemRxiv*, Vol. 1, pp. 1–56, 2019.

50. Liu, Y., C. Li, Z. Ren, S. Yan and M. R. Bryce, "All-organic thermally activated delayed fluorescence materials for organic light-emitting diodes", *Nat. Rev. Mats.*, Vol. 3, p. 18020, 2018.

51. Yu, Y., X. Tang, H. Ge, Y. Yuan, Z. Jiang and L. Liao, "Fluorenone-based thermally activated delayed fluorescence materials for orange-red emission", *Organic Electronics*, Vol. 73, pp. 240–246, 2019.

52. Huang, W., M. Einzinger, T. Zhu, H. S. Chae, S. Jeon, S. Ihn, M. Sim, S. Kim, M. Su, G. Teverovskiy, T. Wu, T. V. Voorhis, T. M. Swager, M. A. Baldo and S. L. Buchwald, "Molecular Design of Deep Blue Thermally Activated Delayed Fluorescence Materials Employing a Homoconjugative Triptycene Scaffold and Dihedral Angle Tuning", *Chem. Mater.*, Vol. 30, pp. 1462–1466, 2018.

53. Bui, T., F. Goubard, M. Ibrahim-Ouali, D. Gigmes and F. Dumur, "Thermally Activated Delayed Fluorescence Emitters for Deep Blue Organic Light Emitting Diodes: A Review of Recent Advances", *Appl. Sci.*, Vol. 8, p. 494, 2018.

54. Kim, J. H., J. H. Yun and J. Y. Lee, "Recent Progress of Highly Efficient Red and Near-Infrared Thermally Activated Delayed Fluorescent Emitters", *Adv. Optical. Mater.*, Vol. 6, p. 1800255, 2018.

55. Wex, B. and B. R. Kaafarani, "Perspective on Carbazole-Based Organic Compounds as Emitters and Hosts in TADF Applications", *J. Mater. Chem. C*, Vol. 5, pp. 8622–8653, 2017.

56. Dias, F. B., K. N. Bourdakos, V. Jankus, K. C. Moss, K. T. Kamtekar, V. Bhalla, J. Santos, M. R. Bryce and A. P. Monkman, "Triplet Harvesting with 100% Efficiency by Way of Thermally Activated Delayed Fluorescence in Charge Transfer OLED Emitters", *Adv. Mater*, Vol. 25, pp. 3707–3714, 2013.

57. Duan, Y., L. Wen, Y. Gao, Y. Wu, L. Zhao, Y. Geng, G. Shan, M. Zhang and Z. Su, "Fluorescence, Phosphorescence, or Delayed Fluorescence?– a Theoretical Exploration on the Reason Why a Series of Similar Organic Molecules Exhibit Different Luminescence Types", *J. Phys. Chem. C*, Vol. 122, pp. 23091–23101, 2018.

58. Huang, R., J. Avo, T. Northey, E. Chaning-Pearce, P. L. Santos, J. S. Ward, P. Data, M. K.Etherington, M. A. Fox, T. J. Penfold, M. N. Berberan-Santos, J. C. Lima, M. R. Bryce and F. B. Dias, "The contributions of molecular vibrations and higher triplet levels to the intersystem crossing mechanism in metal-free organic emitters", *J. Mater. Chem. C*, Vol. 5, pp. 6269–6280, 2017.

59. Li, X., G. Baryshnikov, C. Deng, X. Bao, B. Wu, Y. Zhou, H. Agren and L. Zhu, "A three-dimensional ratiometric sensing strategy on unimolecular fluorescence–thermally activated delayed fluorescence dual emission", *Nat. Commun.*, Vol. 10, pp. 731–739, 2019.

60. Girardon, M., S. Parant, A. Monari, F. Dehez, C. Chipot, E. Rogalska, N. Canilho and A. Pasc, "Triggering tautomerization of curcumin by confinement into liposomes", *ChemPhotoChem*, Vol. 3, pp. 1–9, 2019.

61. Wei, Q., Z. Ge and B. Voit, "Thermally Activated Delayed Fluorescent Polymers: Structures, Properties, and Applications in OLED Devices", *Macromol. Rapid Commun.*, Vol. 40, pp. 1800570 (1–19), 2018.

62. Jhulki, S., M. W. Cooper, S. Barlow and S. R. Marder, "Phosphorescent and TADF polymers and dendrimers in solution-processed self-host organic light-emitting diodes: structure analysis and design perspectives", *Mater. Chem. Front*, Vol. 3, pp. 1699–1721, 2019.